Global Energy, 2023, 29 (1); 52–79.
Глобальная энергия. Том 29, № 1, 2023. С. 52–79.

This article has been previously published. Citation link: M.K. Nazeeruddin, M. Vasilopoulou. Perovskite Solar Cells 3rd Annual Report of the Global Energy Association. pp. 20–48. The original full text of the report is available at the link: https://globalenergyprize.org/en/wp-content/uploads/2022/06/02545_22_brosh_GlobalEnergy_block_preview-2.pdf

M.K. Nazeeruddin[1], M. Vasilopoulou[2]

[1] Institute of Chemical Sciences and Engineering,
École Polytechnique Fédérale de Lausanne (EPFL),
Sion, Switzerland;

[2] Institute of Nanoscience and Nanotechnology,
National Centre for Scientific Research Demokritos,
Attica, Greece

PEROVSKITE SOLAR CELLS

Perovskite solar cells: progress in efficiency and stability

Our modern world is witnessing severe climate changes, which constituents the long overdue transition to alternative energy sources highly imperative. Solar energy is clean and abundant and its usage can limit the consumption of fossil fuels, thus protecting the environment. They convert the sun's energy directly into electricity through the application of semiconductor materials that effectively absorb photons with energy higher than their energy gap values and produce charge carriers. These are then transported through the device and collected in an external circuit through the application of an inverse bias.

Solution-processed organic-inorganic halide perovskite solar cells (PSCs) have recently experienced unprecedented growth, reaching power conversion efficiencies (PCE) exceeding 25%,[1] challenging the widely established silicon solar cells. The detailed analysis of Shockley and Queisser[2] has predicted a 32.5% maximum efficiency for single-junction solar cells based on absorber materials with an optimum bandgap of 1.3 eV.[3] It becomes clear that the performance recently obtained with PSCs is rapidly approaching the theoretical limit. Furthermore, such devices can be incorporated on flexible substrates using solution-based deposition methods suitable for large-area fabrication and, together with their semi-transparency, hold promise for entering niche markets. Their capability to be easily integrated from building facades to small consumer items to fabrics and portable electronics makes now possible the concept of putting solar harvesting devices everywhere, something previously unimagined with the rigid and heavy-weight silicon photovoltaic cells.

PSCs have rapidly evolved since the seminal work by Miyasaka et al.,[4] who exploited organic-inorganic hybrid halide perovskites as sensitizers for visible-light conversion in dye-sensitized solar cells (DSSCs) achieving, however, a modest power conversion efficiency (PCE) of 3.8%. A great breakthrough was made in 2012 by the Graetzel[5] group that reported solar cells based on methylammonium (MA) lead trihalide perovskites with efficiencies > 9%. Similarly to DSSCs, these devices included a mesoporous titanium dioxide (TiO_2) electron transport layer, therefore, termed as mesoscopic PSCs. At the same time, Snaith[6] group introduced the meso-superstructured solar cell architecture employing insulating mesoporous alumina as an inert scaffold for the perovskite film and further increasing the PCE to > 12%. In the following years, the planar PSC architecture using a thin and compact perovskite absorber was introduced.[7–15] Advances in thin film deposition methods using either solution-processing16 or thermal evaporation,[17] allowed their PCEs to rapidly increased and reach the outstanding values reported to date. The fundamental understanding of the basic physical and chemical properties of

© M.K. Nazeeruddin, M. Vasilopoulou, 2023. Published by Peter the Great St. Petersburg Polytechnic University

the perovskite thin film and crystal surfaces, including topics such as electronic structure, crystal imperfections, surface termination and surface reactivity, has also enabled progress in materials and device engineering.[18]

However, a common attribute of these solar technologies is their lack of sufficient evidence of their long-term stability that hinders their commercial viability. In particular, any new solar cell technology must pass the IEC 61646 protocol of stability and lifetime before it becomes commercially available. This protocol includes testing standards, including thermal cycling and freeze tests, along with illumination and damp heat tests.[19,20] In addition, there are economic and marketing standards to be met known as ISOS protocols.[21] These include but are not limited to facile fabrication using low-cost materials and processes.[22,23] All these requirements can be met by judicious material design, sophisticated device engineering and suitable device packaging/encapsulation.[24,25] Intensive research efforts have been focused on interface engineering, the dimensionality and compositional optimization of the perovskite active layer, and thin film deposition process parameters. Also, the developments of all-inorganic compounds for the perovskite absorber and for the interfaces, investigation of passivation materials and approaches that can reduce the surface, interface and bulk defects in perovskites have greatly affected the device performance and stability. These efforts have recently resulted in highly enhanced photovoltaic efficiency and improved long-term stability of PSCs that are now approaching maturity, which will soon enable their impressive market entry.

Device configurations: mesoscopic and planar n-i-p and p-i-n solar cells

Mesoscopic structure. The first reported PSCs had adopted the mesoporous configuration of the dye-sensitized solar cells (DSSC) adapted from solid-state DSSCs in which the dye sensitizer has been replaced by the halide perovskite. These first demonstrations of PSCs were based on the archetypal 3-dimensional (3D) methylammonium lead iodide ($MAPbI_3$) perovskite and yielded PCEs between 6–10%,[26,27] which were significantly improved to over 25%.[28]

In a typical mesoscopic device architecture, a thin (~50 nm) compact layer of TiO_2 is coated on the fluorinated tin oxide (FTO) transparent conductive oxide (TCO), which serves as the electron selective contact on a glass substrate.[28] The mesoporous TiO_2 layer is then printed onto the compact layer to serve as the scaffold for the infiltration of the perovskite absorber as well as the electron transport layer (ETL) (also termed as the electron selective layer, ESL). After sintering at a high temperature (about 450°C), the deposition of the 300–600 nm thick perovskite absorber layer using either solution processing or vacuum deposition is accomplished. The device architecture (shown in Fig. 1a) is completed by the deposition of a thin hole transport layer (HTL) (or else hole selective layer, HSL) capped with a metal electrode (usually gold (Au) or silver (Ag)). The working principle of these devices is based on the absorption of light by perovskite absorber, generation of charge carrier pairs within the absorber layer, charge dissociation and separation, and charge transport to respective electrodes (Fig. 1 b).[29] For high efficiencies, the perovskite absorber should possesses an optimum bandgap of 1.55–1.6 eV and a high absorption coefficient (~10^5 cm^{-1}) so as a maximum portion of the visible light to be absorbed.[30] The transparent TCO and the charge transport layer coated on it should have negligible absorption in order to ensure that most incident light reaches the perovskite absorber where it produces photogenerated electron-hole pairs. These pairs are next dissociated into free charge carriers. The low exciton binding energy of perovskite absorbers (in the range of a few meV[31]) practically results in the generation of free charge carriers. This enables high-efficiency solar cell operation since there is no need for the application of external forces to separate the photogenerated electron-hole pairs.[32] The device performance is also affected by the efficient charge transport within the device layers and extraction towards respective electrodes. Charge selective layers that allow only one type of charge carriers to be extracted at each electrode are hence employed to influence interfacial recombination, charge accumulation and extraction, and consequently to determine the achieved photovoltaic parameters achieved in these devices.

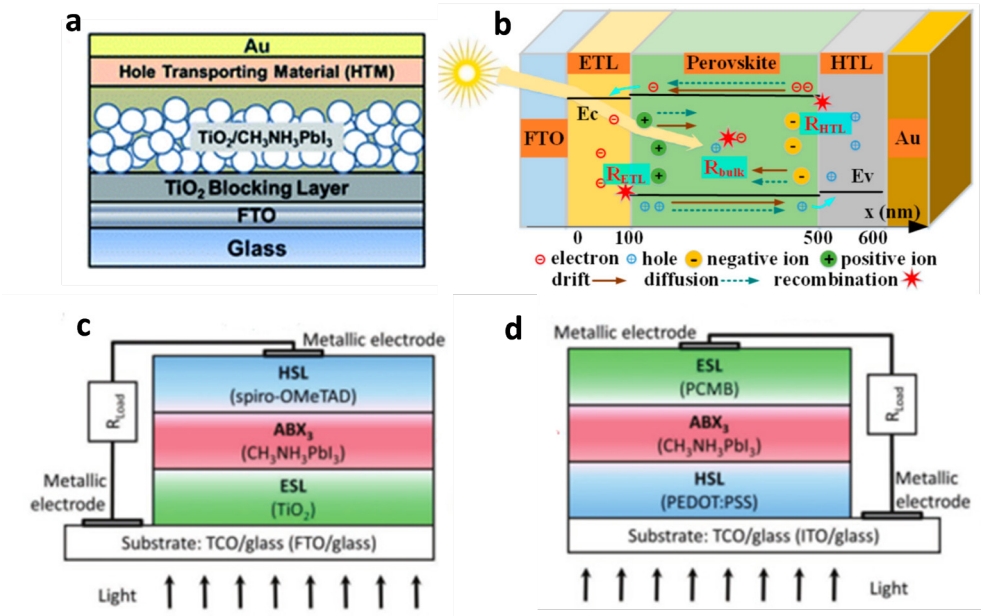

Fig. 1. (a) Typical device architecture of mesoscopic perovskite solar cells. Adapted with permission from Ref. 28 Copyright © 2017 the Royal Society of Chemistry. (b) Schematic of the working principle of perovskite solar cells. Adapted from Ref. 29 under the terms and conditions of the Creative Commons Attribution (CC BY) license. Copyright © 2020 MDPI, Basel, Switzerland. (c) The regular planar (n-i-p) PSC configuration where electrons are collected at the conducting substrate and (d) the inverted planar (p-i-n) architecture where holes are collected at the FTO substrate. Adapted with permission from Ref. 36. Copyright 2018, John Wiley and Sons

Besides the mesoscopic structure using a single mesoporous TiO_2 (or other metal oxide) scaffold, PSCs with a triple layer consisting of two different mesoporous oxides such as TiO_2 and zirconium oxide (ZrO_2), and carbon PSCs, have been successfully demonstrated.[33] In the first demonstration, the device was fully printable, consisting of perovskite that was infiltrated into the porous TiO_2/ZrO_2 scaffold by drop-casting the precursor solution through the printed carbon (C) layer, which served as the top cathode electrode.[33] Despite the fact that this device was free of hole transport layer, it yielded a PCE of 12.84% and good long-term stability. However, it is challenging to control the perovskite crystallization in these devices due to the complicated structure of the triple-layer scaffold.[34]

Planar structure. In recent years, the regular planar (n-i-p) or inverted planar (p-i-n) PSC architectures have dominated due to their simplicity and high efficiencies already achieved. In these structures, the perovskite planar absorber is deposited directly either on the electron transport (n-i-p) or the hole transport (p-i-n) material (Fig. 1 c,d), which transport photogenerated charges towards the anode and cathode contact, respectively.[35,36] As the mesoporous TiO_2 layer is omitted in these planar devices, they can be processed at a temperature below 150°C and therefore are advantageous for mass production.

The regular (n-i-p) planar architecture consists of a bottom transparent electron extracting contact (also termed as the anode), an n-type thin, compact ETL (or else ESL), the perovskite absorber layer, the p-type HTL (or else HSL) and the top metal cathode (which is the hole extracting contact). The most efficient devices are based on a tin oxide (SnO_2) instead of TiO_2 bottom ETL.[37] PSCs with the inverted p-i-n structure have a revere sequence of the ETL and HTL compared to the regular n-i-p structure.[38] In these devices, the bottom HTL is either an organic p-type semiconductor or a p-type transition metal oxide such as tungsten, nickel and copper oxides (WO_x, NiO_x, CuO_x); the latter enabled sufficient rise in efficiency but, most importantly, instability to ambient air.[39–41] Notably, all these device architectures use metal contacts such as gold (Au) or silver (Ag) as the top electrodes.[42,43] However, carbon composite

electrodes can offer an affordable, conductive alternative with abundant sources and blends of carbon black and graphite which are also chemically resistant towards oxidation/reactions, thus acting as protective barriers prohibiting moisture penetration into the perovskite absorber. Furthermore, they can be printed in batch or continuous roll-to-roll processing hence offering the possibility for fully printable large area devices for facile incorporation in substrates of various schemes.[44,45]

Composition and dimensionality of perovskite materials

Composition of perovskite materials. Halide perovskites are materials of the general formula ABX_3, where A-site constitutes of monovalent cations such as organic methylammonium (CH_3NH_3, MA) and formamidinium ($CH(NH_2)_2$, FA) or an inorganic cation such as cesium (Cs) and rubidium (Rb). For B-site occupation, a heavy divalent metal such as lead (Pb) or tin (Sn) is applied and X is a halogen anion (i.e., Cl, Br, I). In this structure, X^- occupies the vertices in $[BX_6]_4^-$ octahedral, which share corners in all three orthogonal directions to generate infinite 3D $[BX_3]^-$ frameworks. The divalent B^{2+} are placed at the centers of these octahedral.[46] The smallest volume enclosed by neighbouring octahedral defines a cuboctahedral cavity and hosts the monovalent cation A^+. Different possible perovskite structures can be regarded as obtained by rotating or distorting the BX_6 octahedra, displacing the B^{2+} metal cations off-center and rotating the A^+ cations within the cuboctahedral cavity. More than one structure is usually found for a perovskite material with a given chemical composition, depending on the temperature and preparation methods. For example, the archetypal $MAPbI_3$ perovskite undergoes phase transformations during cooling from cubic to tetragonal at the temperature of 54°C and from tetragonal to orthorhombic at –111°C (Fig. 2 a–c).[47]

To predict the crystal structure stability of halide perovskites, V.M. Goldschmidt introduced in 1926 the tolerance factor, a, which describes an estimate of the achieved lattice geometry by taking into account the ionic radii of various ions in the structure. The tolerance factor describes the size mismatches that a perovskite structure can tolerate through the formula:

$$\alpha = \frac{r_A + r_X}{\sqrt{2}\left(r_B + r_X\right)}, \quad (1)$$

with r_i being the radii of i = A, B and X ions in the perovskite ABX_3. It has been found that perovskite materials with a tolerance factor of a = 0.9–1.0 are capable of forming an ideal cubic structure; those with a = 0.8–0.9 usually form distorted perovskite structures (usually orthorhombic) consisting of tilted octahedra, while non-perovskite structures are formed when the tolerance factor is above 1 or below 0.8 (Fig. 2 d).[49] The ideal cubic perovskite phase is also denoted as the α-phase and the phase with non-perovskite structures as the δ-phase. Both the performance and stability of PSCs are highly connected with the formation of the black perovskite α-phase. Based on the above considerations, there are only limited possibilities for the A^+ cations that enable tolerance factor values between 0.8 and 1 and stabilize perovskite structures, namely Cs^+, $CH_3NH_3^+$ (MA^+), and $HC(NH_2)_2^+$ (FA^+).

Composition plays a crucial role in determining the stabilization of crystal structure and optoelectronic properties of the resultant material. For example, the archetypal $MAPbI_3$ although it stabilizes to a black quasi-cubic phase upon post-annealing, it decomposes to PbI_2 when exposed to light or moisture; it is also decomposed during annealing at 85°C even in an inert atmosphere.[50–52] $FAPbI_3$ is being advantageous concerning its thermal stability as it is relatively stable up to up to 150°C in air. It also exhibits a beneficial bandgap of 1.48 eV (compared to 1.57 eV for $MAPbI_3$).[53] However, it still suffers from severe structural instability at room temperature as it commonly crystallizes into the yellow hexagonal δ-phase instead of the black photoactive α-phase.[54]

Compositional engineering by intermixing cations or/and halides can combine the advantages of the constituents while avoiding their stability drawbacks. It was demonstrated that even a small amount

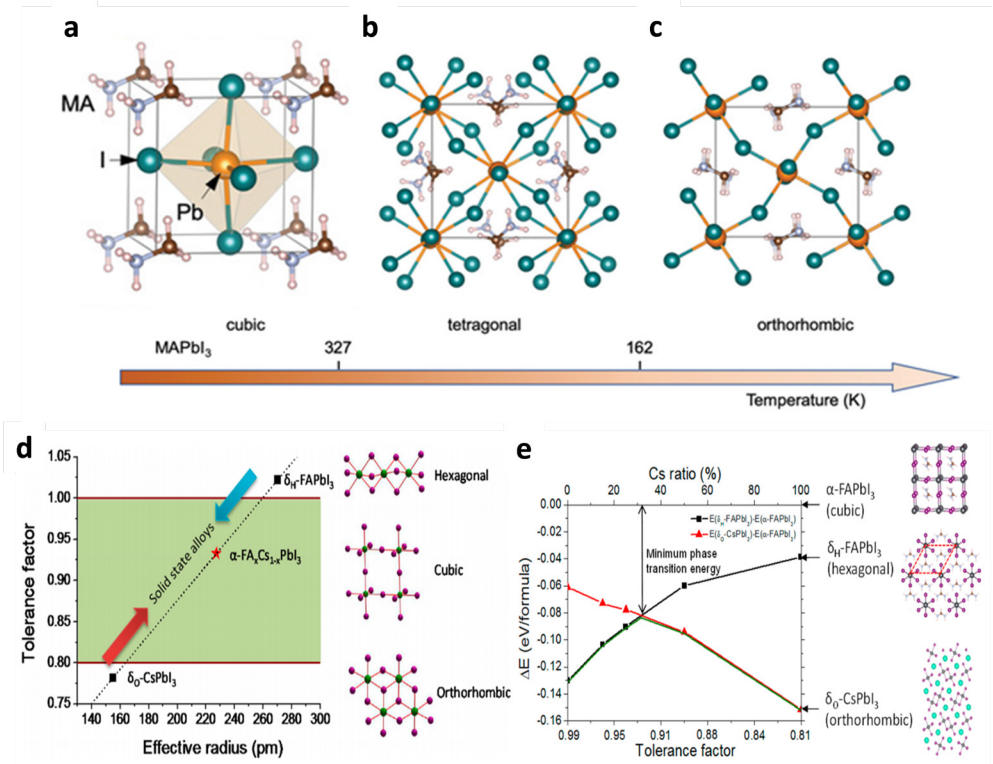

Fig. 2. Crystal structures of the three different MAPbI3 phases: (a) cubic, (b) tetragonal, and (c) orthorhombic phases. The crystal structures of the three phases differ by rotation of the inorganic octahedral cages. The critical temperatures of the phase transitions are marked on the temperature axis. Adapted from Ref. 47. Copyright 2020, John Wiley and Sons. (d) Correlations between tolerance factor and crystal structure of perovskite materials. (e) The calculated energy difference between α-phase and different δ-phases for $FA_{1-x}Cs_xPbI_3$ alloys with different Cs ratios. Adapted with permission from Ref. 49. Copyright 2015, Elsevier

of MA is sufficient to induce a preferable crystallization into the photoactive phase of FA perovskite, resulting in a more thermally and structurally stable composition than the pure MA or FA compounds. This illustrates that the MA can be regarded as a crystallinity stabilizer of the black $FAPbI_3$ perovskite phase. Furthermore, through alloying $FAPbI_3$ with $CsPbI_3$, the effective tolerance factor can be effectively tuned, and the stability of the photoactive α-phase of the mixed perovskite can be significantly enhanced (Fig. 2 e).[49] The substitution of I^- with Br^- in the mixed halide structure leads to the reduction of the lattice constant and a transition from a distorted tetragonal to the cubic perovskite structure with advanced optoelectronic properties.[55–57]

As a step forward, intermixing Cs^+, which has a considerably smaller ion than both MA^+ and FA^+, in a triple cation configuration provides additional versatility in fine-tuning high-quality perovskite materials.[58] Incorporation of sufficient amounts of Cs^+ reduces trap density by one order of magnitude, therefore, decreasing the non-radiative recombination rates and increasing the device efficiency. Notably, the triple cation perovskite films are less affected by temperature for a fixed halide ratio. For example, increased Br- content also contributes to thermal stability. Cs^+ induces black phase formation of FA based perovskites even at room temperature and contributes to better morphology and crystal growth of the perovskite film, which in turn endows the fabricated devices with higher efficiency and long-term stability.

Finally, incorporation of traces of the small radius rubidium (Rb) (r_{Rb+} =152 pm versus r_{Cs+} = = 167 pm) has been recently found to stabilize the black phase of FA perovskites at room temperature. Whereas it is clear from the tolerance factor discussion above that Cs^+ is the only elemental cation that

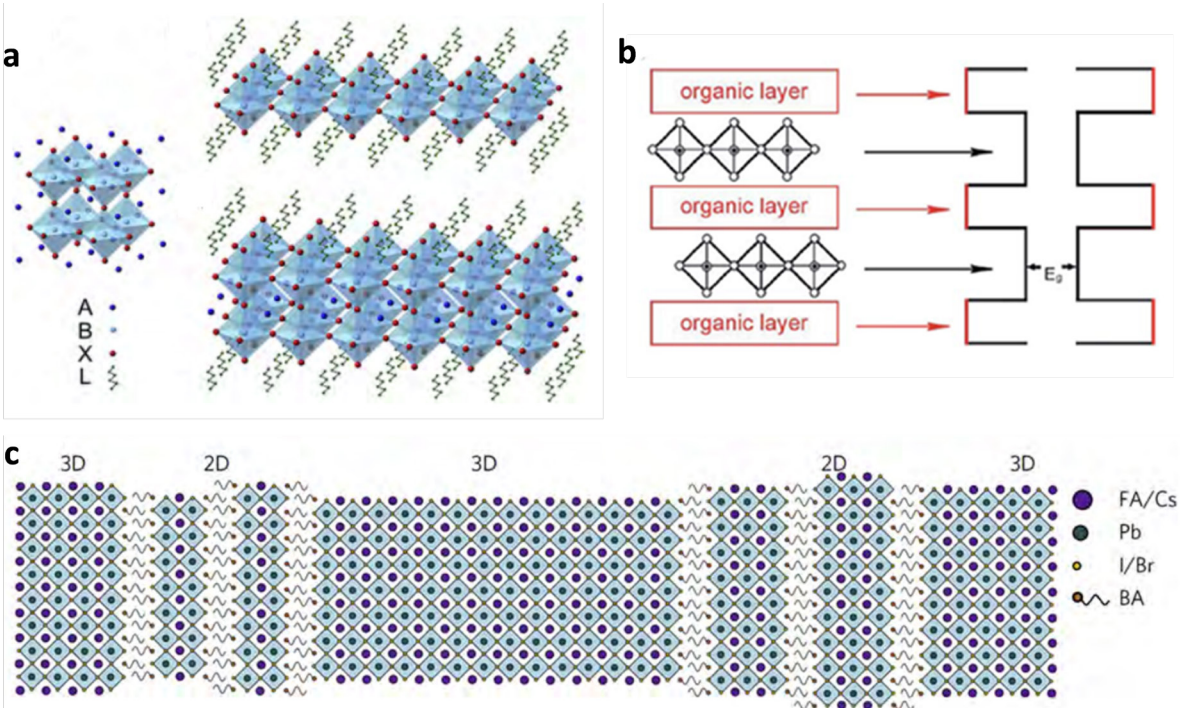

Fig. 3. (a) Illustrative schematic of the crystal structure of different halide perovskite materials. (a) Perovskites with the chemical formula ABX3. RP perovskites with n = 1. RP perovskite with n = 2. The chemical formula of RP perovskites is $L_2A_{n-1}B_nX_{3n+1}$. Reproduced with permission from Ref. 61. Copyright 2019, The Royal Society of Chemistry. (b) The quantum well structure, formed by alternating semiconductor inorganic sheets with organic layers having a wider bandgap. Reproduced with permission from Ref. 63. Copyright 2018, The Royal Society of Chemistry. (e) Schematic illustration of the proposed self-assembled 2D-3D perovskite film structure. Reproduced with permission from Ref. 61. Copyright 2019, The Royal Society of Chemistry

it is large enough to sustain the perovskite structure, Rb^+, despite not being suitable as a pure cation in perovskite compounds, it can still be integrated in small amounts into the mixed-cation structures.[59] Recent studies implied very small non-radiation recombination losses in mixed-cation perovskites with Rb^+ traces owing to very low bulk and surface defect density in these materials.[60] Moreover, it was observed that the charge transport within the RbCsMAFA perovskite layer is substantially faster than in CsMAFA, which is already much more defect-free than MAFA.

Dimensionality of perovskite materials. Besides the widely studied three-dimensional (3D) perovskite structures, low dimensional such as two-, one- and zero-dimensional (2D, 1D, 0D) perovskites have been recently synthesized and studied for their intriguing optoelectronic properties. Those with a 2D structure, also known as Ruddlesden–Popper (RP) layered perovskites, can be described by the formula $L_2A_{n-1}B_nX_{3+1}$ (Fig. 3 a),[61] where L is a large organic cation usually aliphatic or aromatic alkylammonium of the chemical type $R–NH_3$. Representative examples are 2-phenyl ethyl ammonium (PEA) and n-butylammonium (n-BA).[62]

These 2D perovskites consist by conductive $(A_{n-1}B_nX_{3n+1})^{2-}$ sub-layers that derive from the ABX_3 structure; they consist of MX_6 octahedrons that are sandwiched by the sub-layers formed by the insulating organic ligands. The thickness of the perovskite sub-layer, which is defined by the n value (n = 1, 2, 3, 4,), can be adjusted by careful engineering of the stoichiometry to alter the properties of the resultant material.[63,64]

These perovskites generally exhibit superior structural stability arising from the strong van der Waals forces among the organic spacers.[65] Moreover, the large hydrophobic in nature organic ligands serve as buffer layers that protect the perovskite sub-layers from thermal and moisture initiated decomposi-

tion.[66,67] Notably, the organic spacers act as large energy gap quantum wells that prohibition migration which is a significant bottleneck in 3D counterparts (Fig. 3 b).[63,68] However, this multiple quantum well structure of RP perovskites results in weaker visible absorption and lower charge carrier mobility compared to their 3D counterparts.[69–71] Moreover, they present higher exciton binding energies compared to 3D perovskites (in the range of 170–480 meV compared to 40–50 meV), which prohibits direct dissociation of excitons (the excitons in 2D are generally considered as the Wannier-type) to free carriers.[72] Therefore, photogenerated electron-hole pairs are strongly bound with Coulombic attraction in 2D perovskites.[73] This is why the so-called excitonic absorption can be easily observed in these perovskites even at room temperature. It appears as a sharp peak below the bandgap onset. In addition, the low carrier mobility of these perovskites due to the presence of the insulating organic spacers induces charge accumulation and non-radiative recombination at the interface of the conductor/insulator phases and hinders charge transport and extraction.

Because of these unfavorable characteristics, 2D perovskite-based solar cells lag behind in efficiency compared to their 3D counterparts and huge research efforts have been devoted to engineering their composition and optoelectronic properties. These include design of semiconducting p-conjugated organic spacers to tune the mobility of organic sub-layers.[74,75] An attractive approach to tackle the limitations of 2D perovskites is also the combination with 3D structures and fabrication of mixed dimensionality 2D-3D perovskites (Fig, 3 c).[63,76] This can be accomplished by increasing the value of n in the perovskite formula above 10 to prepare materials with properties similar to 3D perovskites yet featuring the 2D structure.[77] In these structures, charges are highly confined to the 3D phase hence overcoming the limitation of trapping and recombination at the perovskite/organic interfaces in the 2D perovskites.[78] As a result, the efficiency of PSCs based on 2D-3D perovskites are highly improved compared to devices fabricated with the 2D structures. Moreover, the presence of the 2D component endows their devices with exceptional stability.[79,80]

Deposition methods: vacuum deposition, solution deposition and printing techniques

The structural and optoelectronic properties of perovskite materials are highly related to the procedure adopted for their preparation. This is because only high-quality films can enable the excellent intrinsic perovskite material characteristics to be fully exploited. A variety of deposition methods have been reported, which can be categorized into vacuum deposition and solution processes.

Vacuum deposition. With the vacuum deposition, the perovskite films are prepared by co-evaporation of two or more precursors (Fig. 4 a). The precursors are sublimated and travel freely from the source towards the substrate surface and deposited onto it. This method produces high-quality perovskite films and high efficiency PSCs.[81] It can be used for the deposition of layered thin films for the fabrication of multiple junction solar cells on top of large substrates.[82] However, it also requires the use of expensive vacuum facilities and increases the device fabrication cost.

The easiest way to employ the thermal chemical evaporation is by a one-step sublimation of the precursor materials on top of the desired substrate. However, this process requires careful adjustment of the quantities and sublimation rate of each reagent in order to achieve the desired stoichiometry of the perovskite film. Another possibility is to prepare the perovskite powder and use it (instead of the precursors) for sublimation.[83] This would allow better control over the stoichiometry of the thin film, which would affect its properties. In both cases, this method offers the deposition of extremely uniform and pinhole-free films of adjusted thickness all over the substrate area.[84,85] Besides co-evaporation of different precursors, sequential evaporation by using dual-source thermal evaporators is also adopted. A major advantage of this sequential method is the full surface coverage and high crystallization phase purity, as well as the highly smooth surface of the resultant perovskite films.[86] In spite of the exceptionally uniform films and the high reproducibility that this technique offers, the cost of the infrastructure required for the perovskite formation is a bottleneck for use in a larger scale.

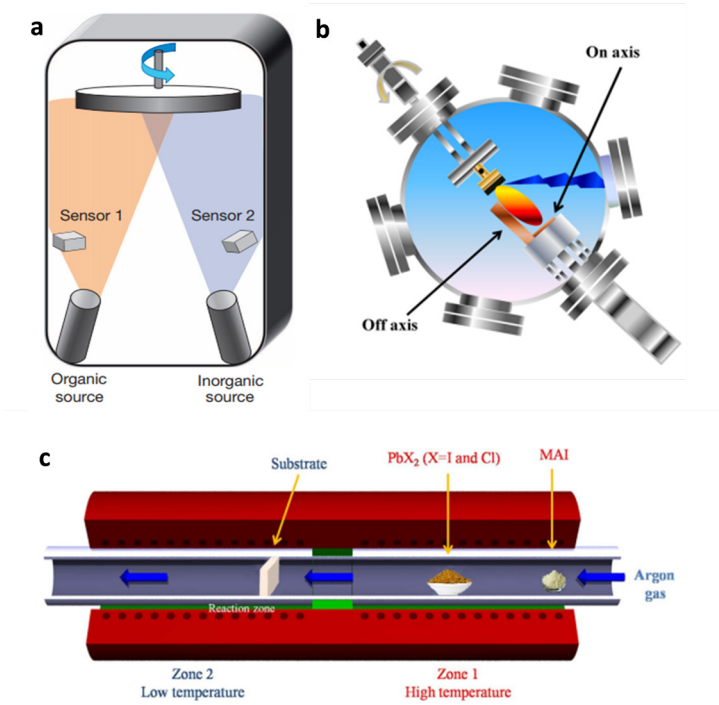

Fig. 4. (a) Schematics of a dual-source evaporation for vacuum deposition of perovskite films. (b) On-axis and off-axis fabrication of thin films through PLD. Reproduced with permission from Ref. 89 Copyright 2020, American Chemical Society. (c) Schematic fabrication of perovskite (i.e., $MAPbI_3$) thin film through CVD. Reproduced with permission from Ref. 92. Copyright 2014, The Royal Society of Chemistry

Pulse laser deposition (PLD) is another vacuum deposition method in which the precursor material is subjected to a pulsed laser beam of high energy while being inside the high vacuum chamber. In this way, the laser vaporizes the target material almost instantly, thus creating a plasma plume which is deposited as a thin layer onto the desired substrate. The substrate can be either perpendicular (on-axis deposition) or parallel to the plasma plume (off-axis deposition) (Fig. 4 b).[87] The solid precursors can be kept at room temperature during the deposition and the plasma energy source is placed outside the vacuum chamber, making this method quite simple compared to other vacuum methodologies. At the same time, the superior quality of the crystalline layers could be attributed to the high energy of the impacting ions.[88,89] However, possible disadvantage of PLD could be the different vaporization rate of each moiety, which in turn affects their deposition and the composition of the formulated film. For example, the organic moiety creates a smoother surface on the film, because of its easy volatilization through plasma, while the inorganic moiety has a different morphology due to a different forming path, thus creating inhomogeneous areas on the substrate. This is why the target material should not stoichiometric but its organic part is in excess.

In vacuum chemical vapor deposition (CVD), the volatile precursors that form the perovskite film are generated and then injected from the main gas flow into a quartz chamber under vacuum conditions. In the chamber, gas-phase reactions take place, forming intermediate products, which are then deposited on top of the substrates. The precursors are adsorbed onto the substrate surface, followed by diffusion of the reagents, nucleation and crystal growth, with the final result being the formation of the perovskite film. During the film formation, the precursors can either react or decompose. Any volatile byproducts formed during the reaction are desorbed and transferred to the main flow.[90] When the pressure conditions during the reaction are taken into consideration, the CVD techniques can be categorized as atmos-

pheric pressure CVD (APCVD), low-pressure CVD (LPCVD) and ultrahigh vacuum CVD (UHVCVD). If the gas phase is taken into consideration, the technique can have as subcategories the metal-organic chemical vapor deposition (MOCVD), aerosol assisted CVD (AACVD), direct liquid injection CVD (DLICVD), and hybrid physical CVD (HPCVD).[91] The easiest way of categorization, however, is by one-step and two-step methodology.

During the one-step deposition, the organic and inorganic moieties in the gas phase are simultaneously injected into the vacuum chamber, are co-evaporated and adsorbed on the preheated substrate. This method is quite helpful since no secondary evaporation step is necessary and is a gas-only method. However, this method can also be applied in the case of mixed halide perovskites, producing pinhole-free films.[92] In this case, the differences in vaporization time should be taken into consideration. In the case of the two-step deposition, each moiety is deposited separately on the substrate. This allows full control over the final film thickness and stoichiometry.[93,94] The two-step chemical vapor deposition can also be combined with the metal-alloying technique in order to control the film morphology. The engineering of the alloy composition enhances the quality of perovskite films through large-sized grains in the uniform film.

Solution deposition. In the early attempts, solution deposition was sufficiently accomplished in a single step using a common solution of PbI_2 and MAI precursors (Fig. 5 a).[95] However, the lack of suitable solvents that can dissolve both components and the high perovskite reaction rate resulted in large morphological variations and therefore, to large deviations in the achieved efficiencies. In 2013, Grätzel and co-workers described a sequential deposition method for the successful infiltration of the perovskite pigment within the porous of TiO_2 film (Fig. 4 b).[96] In particular, lead iodide (PbI_2) was first introduced via spin coating from solution into the nanoporous TiO_2 film and subsequently dipped to a solution of methyl ammonium iodide (MAI) to synthesize the resultant $MAPbI_3$ perovskite film. It was found that the conversion to perovskite occurred within the nanoporous oxide as soon as the two precursors came into contact, hence allowing for better control over the morphology and reproducibility of perovskite films.

The most widely used technique for the fabrication of PSCs in the laboratory scale is spin-coating. It can be either a one-step or a two-step deposition method that is characterized as a solution-processing based one. The main advantages of this method are its simplicity, as well as its low cost. During the one-step process, the organic halides along with the metal halides are mixed with an appropriate solvent forming the precursor solution. Mostly aprotic polar solvents are used, such as N,N-dimethylformamide (DMF), dimethyl sulfoxide (DMSO), γ-butyrolactone (GBL), 2-methoxyethanol (2-ME) and acetonitrile (ACN), which exhibit high boiling point and low vapor pressure when at room temperature. The solution formed is subsequently deposited on the substrate surface on top of the ETL in standard architecture solar cells. This substrate is placed on a spin-coater and spun at high rotational speeds for a couple of seconds so that the excess solvent evaporates. During the evaporation, the formation of the perovskite layers takes place, with crystals being formed and grown due to ionic interaction between metal cations and halogen anions. The substrate is finally annealed at a temperature between 80 and 150°C for 10 minutes to 2 hours so that the rest of the solvent is removed.

A similar technique to this is hot casting, during which the mixture of the organic and inorganic solutes is firstly heated at 70°C and subsequently deposited on an already heated substrate at 180°C (Fig. 5 c).[97] The substrate is then put in a spin-coater and finally annealed on a hot plate, which leads to the development of millimeter-scale crystallites. Drop casting is another solution-based deposition method for perovskite films.[98] The main advantages of this method are its low cost and ease of execution. During this method, the perovskite solution containing both the organic and the inorganic moieties is deposited into a substrate with the help of a pipette. This is followed by heating the substrate in a hotplate so that the solvent can be evaporated, thus forming the film. Nonetheless, the thickness, morphology and optoelectronic properties of the perovskite film are highly dependent on the concentration

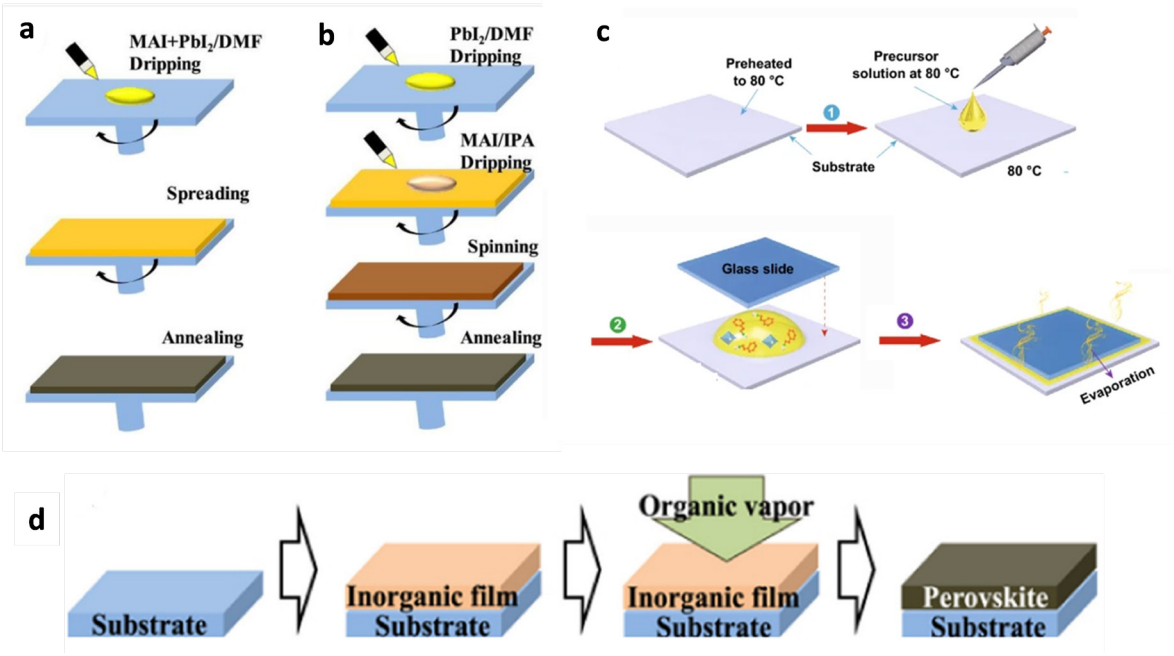

Fig. 5. (a) One-step and (b) two-step deposition of perovskite layer on top of substrate. Reproduced with permission from Ref. 96. Copyright 2018, Elsevier. (c) Schematic illustration of the hot casting process. Reproduced with permission from Ref. 97. Copyright 2020, Springer Nature. (d) VASP deposition method. Reproduced with permission from Ref. 95. Copyright 2018, Elsevier

of the solution, its viscosity and the rate of evaporation of the solvent while on the substrate since no spinning is performed.

Vacuum and solution processes constitute two dominant fabrication techniques for perovskite films. Nevertheless, although vacuum-based environment processes, where the inorganic and organic compounds (i.e PbX_2 and MAX, respectively) serve as the vapor source, provide high-quality films with respectable features, they also lead to time consuming deposition steps and costlier equipment. On the other hand, while the fabrication of a perovskite film via any solution process appears as an alternative approach due to the simple concept that both materials can rapidly form from their solution phase reaction after annealing, undesired pinholes may occur across the whole film.[98,99] Thus, a different deposition technique is developed called Vapor Assisted Solution Process (VASP) that combines both processes' advantageous characteristics (Fig. 5 d).[95,100] VASP is considered to be a modified two-step sequential solution deposition process in which the second step is replaced by a gas-phase reaction. According to this technique, the evolution of the film starts with the construction of the inorganic framework of the perovskite material by a solution process and subsequently, an in situ reaction between the inorganic species and the desired organic vapors takes place, forming the perovskite film.[101] A crucial factor to the formation of the film is the source temperature that creates the appropriate vapor pressure so as not to damage or decompose the gaseous halides salts completely. The substrate temperature will also affect the dynamics of the perovskite formation. In other words, VASP exploits the kinetic reactivity of the organic vapor and the thermodynamic stability of perovskite during the in situ growth process. Hence, the advantage this technique holds over pure vacuum and solution processing is the intercalation of the organic components into the inorganic framework through vapor, as it prevents the high growth rate of the perovskite material during the co-deposition of precursors as well as possible degradation of the inorganic framework upon dipping into an organic solution. Summarizing, VASP can provide perovskite films with full substrate coverage, small surface roughness and well-defined grain sizes up to microscale.

Hydrothermal synthesis is also applied for perovskite films formation. It has emerged as a frontline technology for single crystal growth and metal leaching.[102,103] Hydrothermal synthesis is regarded the synthesis of substances by chemical reactions in a sealed, heated aqueous solution at an appropriate temperature (100–1000 °C) and pressure (1–100 MPa).[104] According to reaction temperature, hydrothermal synthesis is classified into two categories: subcritical and supercritical synthesis reaction. A subcritical synthesis reaction is carried out in the temperature range of 100–240 °C, while supercritical synthesis reaction occurs for much higher temperatures. In addition, according to the vapor pressure of the main composition in the reaction, either low-pressure or high-pressure conditions can be employed to control the morphological features of the as-made materials. The uniqueness of this technique stems from the fact that any stable precursor used in the process can break at a relatively low temperature, thus preventing the extensive agglomeration that solid-state reactions generally cause under high sintering temperatures. Given the fact that hydrothermal synthesis permits rapid mixing of precursors for homogeneous products with controllable parameters; it has become one of the most preferable and adaptable chemical routes to prepare homogeneous perovskite films.

Like hydrothermal synthesis, solvothermal synthesis is a solution reaction-based procedure used for perovskite deposition.[105,106] The difference between the two techniques is that instead of water, in solvothermal synthesis, the primary solvent is usually an organic one. The implementation of solvothermal synthesis, whereby an often homogeneous mixture of liquid and solid precursors are heated in a sealed reaction vessel close or above the boiling point of the main solvent, is particularly well known for the preparation of crystalline materials. Solvothermal synthesis constitutes a versatile alternative to calcinations for developing under milder temperatures metal-organic framework structures such as perovskites. Nevertheless, controlling crystal morphology in terms of particle shape and size is challenging when using solvothermal synthesis.

One of the most effective ways to form better crystals is by temperature tuning. Several approaches of synthetic protocols have been proposed for hybrid perovskites ranging from two-step processes to direct crystallization. Although perovskites have the merit of being deposited from their precursors into a thin film by solution-based processes, it is rather difficult to gain control over the nucleation and crystallization of the as-prepared film from a saturated solution by evaporation of the solvent. The procedure of crystallization is affected by a number of variables like an oxygen-rich atmosphere and humidity that may cause a compounding of crystal sizes and surface chemistries.[107] Both chemical and physical properties can be adjusted at atomic level via the use of reactants and thermal annealing. The most popular procedure to initiate crystallization of perovskite film is thermal annealing at 100°C for 10 min.[108] It has been shown that the microwave irradiation process can lead to a faster and with less energy crystallization of the perovskite material.[109] However, prolonged exposure to microwave irradiation will lead to the opposite result.

Printing techniques. Large area fabrication of perovskite films can be accomplished by suitable printing methods.[110] There are generally two printing processes applied the continuous inkjet printing and the drop on demand inkjet printing. In continuous inkjet printing, the printed perovskite films are generated from a continuous stream under pressure and then ejected from a nozzle that is placed in a potential (Fig. 6 a). As the steam moves out of the nozzle, it transforms into a droplet that moves towards the substrate under the gravity influence. As the droplets fall, they pass through electrodes which charge each one of them. Afterwards, two deflection plates are used in order to correct the trajectory of the majority of the droplets and finally hit the substrate. A piezoelectric transducer (PZT) is also used to create a small pressure fluctuation to the liquid and synchronize the droplet formation. The most important advantage of continuous inkjet printing is the absence of physical contact with the substrate. This is very important as it is possible to print on curved surfaces, rough surfaces and surfaces sensitive to pressure. One of the important disadvantages of this method is that a considerable amount of ink goes to waste. However, these unwanted droplets can be collected in a gutter and recycled to become inkjet material.

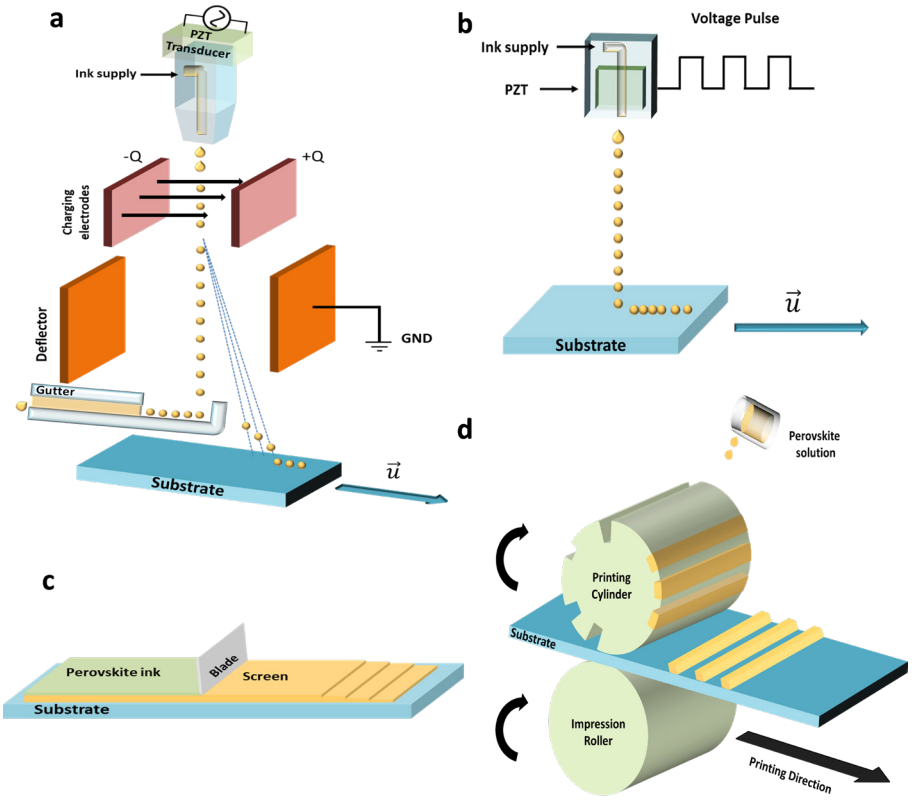

Fig. 6. (a) Illustration of the continuous inkjet deposition method.
(b) Illustration of the Drop-on-demand inkjet deposition method.
(c) Illustration of the screen-printing deposition method. (d) Illustration of the gravure printing technique

In drop on demand method (Fig. 6 b), the printer head can move and shoot the droplets to the desired location or the substrate moves, like previously. For the ejection of the droplets, a regular pulse is generated to the PZT, in the nozzle, and this forces the ink out. Specifically, a cyclic deformation of the piezoelectric transducer occurs due to the impulse current, which causes the droplets to fall from the nozzle.

Screen printing is a commonly used deposition method for which a screen is used to coat the ink onto a substrate (Fig. 6 c). The printing patterns are fabricated due to the open mesh apertures of the screen. A paste is placed on the non-printed areas and the blade is moved across the screen surfaces while it also fills the open mesh apertures with paste. Then, paste in the open mesh is pumped to the substrate. The non-printed areas are resistant to the paste, due to a blocking stencil. As the blade moves toward the screen rear, the tension of the mesh pulls the mesh up away from the substrate. The screen printing technique is used for large deposition areas (several m^2) and the material utilization reaches 100% for a continuous process. This method is also a low-cost method that fabricates several solar cells on a substrate with low fabrication cost but the reproducibility is difficult taking into account the great dependence of the solar cells to the ink properties and the blade force on the screen.

Finally, blade coating, slot-die coating, spray coating and gravure printing can also be applied for the fabrication of large-area perovskite modules.[111] In blade coating, the coating solution is placed in front of a blade which is placed at a fixed distance from the surface that needs to be covered; the blade is moved across in-line with the surface, creating a perovskite film. In slot-die, the perovskite precursor is coated onto the surface of the substrate through a precise coating head whereas in spray coating the precursor is sprayed onto the substrate to deposit the perovskite film. In gravure printing, the ink is applied to an engraved printing cylinder and then it is placed on the substrate (Fig. 6 d). The printing process

goes as follows: The printing cylinder, which has an engraved pattern, is filled with the perovskite ink and then it is placed on the substrate. In order to remove the excess ink from the inactive area of the printing cylinder, a doctor blade is often used. Then, the ink is transferred from the cylinder to the substrate by applying a specific pressure through the impression roller. Unlike the other printing methods, gravure printing deposits and patterns the desired layer at once, with high precision and resolution and in a short time. Also, this technique can also create complex 2D patterns.

Charge transporting materials: Electron transporting materials, hole transporting materials, a dopant-free hole transporting materials and hole conductor-free with carbon counter electrodes

Perovskite solar cells have achieved impressive performance due to progress made in the perovskite absorber and the charge transport and interfacial materials used in the device configuration. In fact, the interfaces between the perovskite film and the charge transport layers are among the most important factors that determine both the efficiency and stability of planar and mesoscopic PSCs.[112] The most critical aspects of such materials that govern the performance of the complete device include possible chemical interactions between those materials and perovskite absorber, the energy level alignment at the interfaces, the charge transport properties of the interlayers and charge recombination therein and so on. Various design strategies for the interfaces and the interfacial materials have been proposed and enabled efficient and stable device operation.[113]

Electron transporting materials. The first PSCs adopted the mesoscopic structure where the perovskite absorber was infiltrated within the TiO_2 mesoporous oxide that served as a scaffold as well as the electron transport layer (ETL), while also blocking the photogenerated holes from reaching the electron selective contact.[114] TiO_2 exhibits high transparency, good electron mobility, well-matched energy levels with those of perovskite and ease of fabrication which render it an excellent choice for mesoscopic PSCs.[115] It appears in the anatase, brookite and rutile phases, dependent on the fabrication procedure, with the anatase to be the most effective amongst the three phases for application in PSCs.[116] However, the commonly used anatase phase generally possesses lower mobility compared with the rutile one,[117] an implication leading to lower short-circuit current (J_{SC}), although with higher open-circuit voltage (V_{OC}), achieved in the anatase based devices.

To increase the mobility of TiO_2, doping with metal or halogen atoms has been widely adopted. Niobium (Nb), lithium (Li), magnesium (Mg), tin (Sn), zinc (Zn), yttrium (Y), zirconium (Zr), and molybdenum (Mo) have successfully been used as doping elements for the planar and mesoporous TiO_2 ETL.[118–122] Moreover, graphene has been successfully used as a dopant for TiO_2 due to the excellent electron transport capability of the former, which helps to improve the electron collection efficiency of the corresponding PSC.[123] In addition, surface modification of the ETL has also been applied to passivate surface defects and reduce interface recombination. Ultrathin interlayers of alumina (Al_2O_3) or titanium nitride (TiN) have been deposited with atomic layer deposition (ALD) and significantly improved the interface properties but also the optical and morphological properties of the perovskite absorber coated on top of it.[124,125] In addition, various organic materials such as amino acids,[126] thiols,[127] and fullerenes,[128] have been used as TiO_2 modifiers facilitating the perovskite crystal growth and enhancing the device performance and long-term stability.

Due to its higher electron mobility compared with TiO_2 and low crystallization temperature, zinc oxide (ZnO) is another widely applied ETL in PSCs.[129] Similarly to TiO_2, doping and interfacial modification can further improve its properties to enable fast extraction rates in PSCs. For example, Al-doped (AZO),[130] and nitrogen (N)-doped[131] ZnO nanorods exhibit reduced work function (W_F) and improved electron transport compared to the undoped ZnO resulting in efficiency enhancement in PSCs. Furthermore, treatment with amino functionalized organic compounds has proven beneficial as it induced the formation of negative interfacial barriers thus reducing the electron extraction barrier towards the anode contact.[132,133]

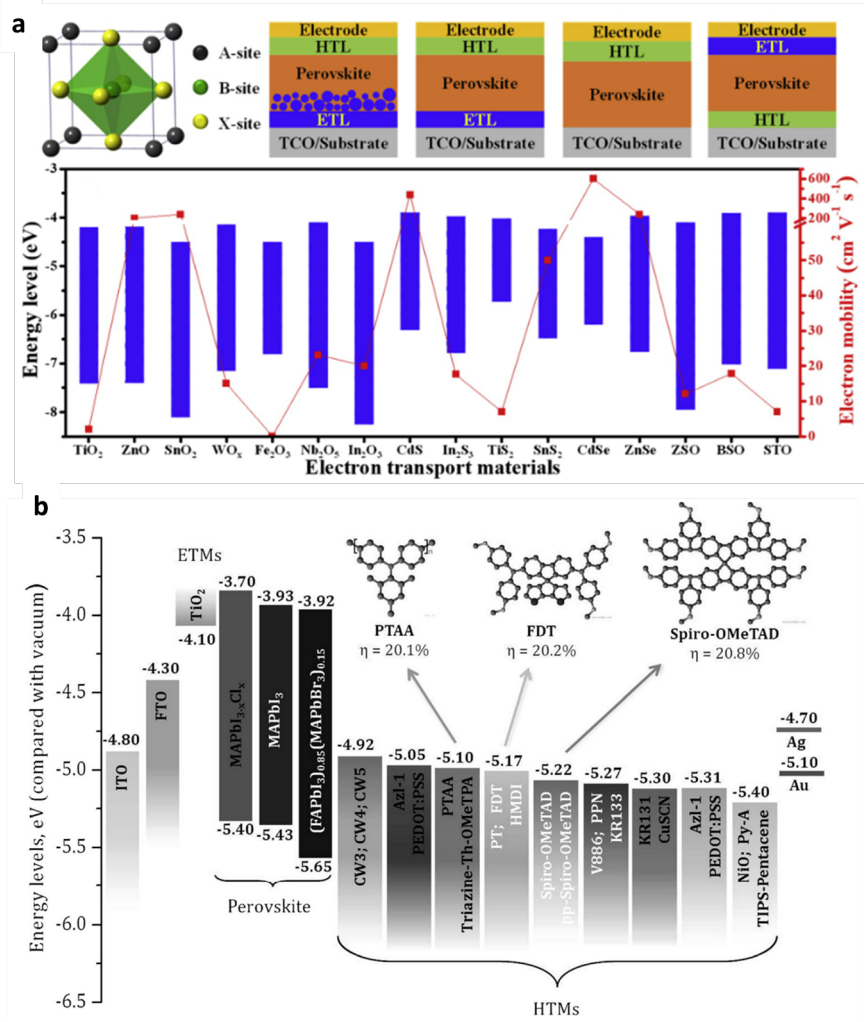

Fig. 7. (a) The crystal structure of perovskites. Structure diagrams of n-i-p mesoscopic, n-i-p planar TCO-ETL PSCs and p-i-n inverted PSCs (top). Electron mobility and band structure of various electron transport materials (bottom). Reproduced with permission from Ref. 142. Copyright 2020, Elsevier. (b) Schematic energy-level diagram of the components used in PSCs, including the most efficient perovskite light absorbers and the best-performing HTLs along with their HOMO levels. Reproduced with permission from Ref. 145. Copyright 2016, John Wiley and Sons

Tin oxide (SnO_2) has been the most established ETL in planar PSCs with the regular architecture.[134–138] It exhibits high transparency in the visible range and favorable energy level alignment with the perovskite absorber. Doping of SnO_2 has been proven beneficial for the stable operation of PSCs. For example, Al-doping reduces the recombination losses originating by the trap states present on the surface of pristine SnO_2 and improves the PCE compared with the undoped ETL-based device.[139] Furthermore, lanthanide (Ln) ions have recently enabled significant performance boosts in perovskite devices using SnO_2 ETLs doped with these materials. In particular, PSCs using yttrium (Y)-doped SnO_2 layers presented high efficiency combined with negligible hysteresis, while the device with the undoped oxide presented inferior performance.[140] Furthermore, surface modification of SnO_2 using, for example, polyethylene glycol (PEG) resulted in improved morphology of the oxide layer and better performance of the resultant PSC.[141]

Recently, several other metal oxides, ternary metal oxides and transition metal dichalcogenides (TMDs) have been also employed as ETL in PSCs due to their attractive electron mobility and energy levels (Fig. 7 a).[142] A precise control over the photoelectric properties of these ETLs achieved by modi-

fied their deposition protocols and probing of the charge dynamics at the interface has led to enhanced performance of PSCs with the additional merit of long-term stability.[143,144]

Hole transporting materials. Hole transporting materials are also indispensable in achieving high photovoltaic performance and stability as they facilitate hole extraction and block the photogenerated electrons simultaneously from reaching the cathode (Fig. 7 b).[145] A large variety of organic and inorganic materials have been applied as HTLs in PSCs. Among them, Spiro-OMeTAD (2,20,7,70-Tetrakis-(N,N-di-4-methoxypheny lamino)-9,9-spirobifluorene) is the most commonly used.[145] It enables fast hole transport under the requirement of sufficient doping to increase its low conductivity. This can be accomplished by using additives in the pristine solution, with the most common to be TBP (4-tert-butylpyridine) and Li-TFSI (lithium bis(trifluoromethylsulfonyl)).[146] However, Spiro-acridine-fluorene and methoxyl (–OMe) substituted (in the para-, meta-, and ortho- positions) Spiro-OMeTAD derivatives have demonstrated efficient device performance with no requirements for additional doing.[147] Moreover, thiophene-based materials have proven efficient HTLs due to their charge extraction capability as revealed from steady-state and time-resolved photoluminescence measurements.[148] In addition, organic compounds using thieno[3,2-b] thiophen conjugated moieties or π-conjugated thiophene bridges attained enhanced PSC performance, even higher than that of the Spiro-MeOTAD based reference device.[149,150]

Poly(triarylamine) (PTAA) the selection choice for the HTL in inverted PSCs.[151–154] One of the highest efficiencies in PTAA-based PSCs was obtained when applying p-doping of PTAA HTM with Li-TFSI and TBP.[152] However, despite the attractive electrical parameters of the fabricated device, p-doping of PTAA HTL has also led to faster degradation of the cell. Generally, PTAA enables stable operation when processed from chlorobenzene or toluene solvents, with the latter to be considered as the more effective in improving the PTAA solubility and thus the film quality of the HTL. However, the successful use of PTAA HTM in PSCs, significant differences in the device performance have been demonstrated dependent on the molecular weight of this polymer. PTAA's molecular weight severely affects the interfacial charge carrier losses in the cell, and it was found that reduced charge recombination rates are obtained when using high molecular weight PTAA.[153] Notably, this polymer exhibits a highly hydrophobic surface after the required post-annealing treatment which deteriorates the quality of the perovskite overlayer.[154] To overcome this bottleneck, short duration oxygen plasma treatment or surface treatment with a DMF solvent have been successfully adopted.[155]

Moreover, dopant-free triarylamine-substituted spiro-cyclopentadithiophene (Spiro-CPDT) based materials have successfully applied as dopant-free HTLs in PSCs.[156] Moreover, materials based on thieno[3,2-b]thiophen conjugated moiety as central unit have also demonstrated capacity for application as dopant-free HTMs.[157] Similarly, star-shaped molecules embedding carbazole or triazine derivatives have been applied as HTLs to PSCs with no use of additives or dopants and enabled comparable performance with devices using the Spiro-OMeTAD.[158] These molecules exhibit high hole mobility, appropriate highest occupied molecular orbital (HOMO) energy level and good film-forming properties on top of the perovskite absorber, properties that are highly beneficial to the device performance.[159]

Metal oxides represent attractive alternatives to organic HTLs due to their resilience to moisture and good thermal and chemical stability. Nickel oxide (NiO) has been widely employed employed as HTL in PSCs reporting a high efficiencies combined with negligible hysteresis.[160] Moreover, nickel cobalt oxide ($NiCo_2O_4$) layers have been incorporated between the Spiro-OMeTAD and the Au anode resulted in excellent device performance with highly improved stability due to the protection that it offered to the hydroscopic Spiro-MeOTAD.[161] Copper thiocyanate (CuSCN) represents one of the most widely studied inorganic HTMs in planar PSCs with the regular architecture.[162] Besides its use as interfacial material, it has also proven beneficial as an additive to the perovskite absorber.[163] By adding CuSCN to the perovskite precursor solution, a bulk heterojunction was formed, which allowed the faster extraction of holes in the perovskite towards the carbon counter electrode in mesoscopic hole transport material-free PSCs, which led to an increased PCE and decreased hysteresis.

Compositional and interface engineering approaches for efficiency stabilization of perovskite solar cells

Organic–inorganic halide perovskites are defect tolerant materials owing to the anti-bonding character of their valence band maximum (that consists of halogen p orbitals, in particular, Cl 3p, Br 4p or I 5p, with a small contribution from the Pb 6s) and conduction band minimum (which is mainly composed of Pb 6p orbitals with a small contribution from the anti-bonding halogen p*). Still, they exhibit a diversity of defects that are encountered in their surface and at grain boundaries (GBs) and can be classified into: halide anion (such as Cl-, Br- and I-) and organic cation (such as MA^+ and FA^+) vacancies, under-coordinated lead cations (Pb^{2+}) and halide anions, lead-halide antisite defects, mobile halide and MA ions, Pb clusters, halide-excess and Pb-halogen antisites. Furthermore, many of these defects form deep trap states, which act as non-radiative recombination centers for the photogenerated charge carriers thus compromising the device efficiency and stability. Passivation of bulk, surface and GB defects is therefore imperative to maximize and, importantly, stabilize the solar cell efficiency. In this context, various passivation and engineering approaches targeting to minimize defect density and, consequently, charge trapping at these defects are widely applied.

Engineering of stoichiometry

The stoichiometry of the perovskite material, regardless of its composition, i.e., single or mixed cation and/or mixed halide, is known to govern the optoelectronic properties of the film and the device performance. For example, it has been shown that non-stoichiometric perovskites may exhibit better properties than the stoichiometric counterparts i.e., an excess of 5% of lead iodide (PbI_2) precursor in the perovskite solution can favorably impact the device performance and stability.[164] Similarly, a small excess of caesium iodide (CsI) in the precursor solution (CsI:Sn_2 1.25:1.0 instead of 1.0:1.0) for the preparation of inorganic caesium tin iodide ($CsSnI_3$) perovskite may significantly boost the device performance through suppressing the undesired oxidation of Sn^{2+} to Sn^{4+} hence avoiding the perovskite doping with an excess of holes.[165] Similarly, the stoichiometry of the reactants and the duration of the second step significantly affects the perovskite film morphology and optoelectronic properties when applying a two-step synthesis involving first the deposition of PbI_2 and afterwards the spin-coating of organic salt solution like methylammonium or formamidinium iodide (MAI/FAI) to form the perovskite film.[166] In particular, sub-stoichiometric PbI_2 and the short duration of the second step usually result to incomplete conversion with some lead iodine residue remaining to the final product. Since the reaction between PbI_2 and the organic salt begins from the top side of the already formed PbI_2 film, short duration of the second step results to the incomplete transformation of the PbI_2 layer to perovskite (especially if this layer is quite thick) with PbI_2 residue to be accumulated at the underlying charge transport layer causing electronic insulation and poor device performance.[167] Notably, small amounts of PbI_2 can benefit the charge collection and transport from the perovskite layer to the corresponding electrode in both, forward and inverted cell architectures since it can passivate surface defects, enhance electron transport and block hole leakage (in forward device architectures) or it can improve hole injection and electron blocking (in inverted structures).[168] In any case, control over the thickness of remaining at the interfaces is imperative for efficient device performance.

The GBs of the perovskite film are also sub-stoichiometric compared to the bulk due to the dangling bonds and non-terminated surface. This deviation from stoichiometry results to the formation of defect states which negatively impact the device performance. Moreover, GBs are potential paths for ion migration within the perovskite matrix, which is generally considered as the main source of hysteresis and instability for the perovskite optoelectronics.[169] In general, the synthetic procedure followed strongly influences the stoichiometry, film forming and optoelectronic properties of the resultant perovskite layer,[170] which has important implication in the fabricated PSCs.

Cation optimization

Methyl ammonium –based perovskites, such as the archetypal $MAPbI_3$ with a bandgap of 1.55 eV, have been the most intensively studied absorber in PSCs. However, they also undergo severe phase transition at 55°C and thermal degradation at 85°C, which necessitates the replacement of MA^+ cation with more stable ones such as the larger FA^+.[171] Mixed cation MAFA-based or even single cation perovskites such as $FAPbI_3$ are shown great potential as alternative perovskite materials with superior thermal stability.[172] Moreover, $FAPbI_3$ presents broader absorption due to its narrower bandgap of 1.48 eV.[173] However, the large size of FA^+ causes lattice distortion thereby affecting the crystal structure of the obtained perovskite material which requires thermal annealing at elevated temperatures in order for the black perovskite α-phase to be stabilized. Mixed cation (MA/FA) perovskites are more easily stabilized at room temperature.[174] Besides FA and mixtures with MA, the high efficiency of a Pb-free PSC was obtained with A-site substitution using a non-polar material bearing the guanidinium (GA^+) organic cation. GA^+ was added in varying ratios into the crystal structure of the $FASnI_3$ along with 1% ethylenediammonium diiodide ($EDAI_2$) to form $GA_xFA_{1-x-2y}SnI_{3-y}EDAI_2$.[175] The optimised device performance was attributed to the presence of $EDAI_2$, which passivated surface defects, controlled the film morphology, and suppressed the Sn^{2+} oxidation to Sn^{4+}. Moreover, the GA co-cation, which has a zero electric-dipolar moment, inside the $FASnI_3$ framework delayed the oxidation of perovskite in the presence of moisture.

Furthermore, monovalent alkali cations such as Cs and Rb have been implemented for substitution in the A-site since their ionic radii fulfill the criteria of Goldschmidt's empirical tolerance factor ($0.8 < t < 1$) to retain the 3D perovskite structure. Cs^+ has been widely incorporated with either MA^+ or FA^+ or a mixture of both at the A-site in multi-cation perovskites along with the aim to alleviate the problem of undesired phase transition and improve their photo- and moisture sustainability.[176] The A-site substitution of Cs^+ shrinks the cubo-octahedral volume of the perovskite crystal lattice, thereof inducing stronger chemical interaction between FA^+ and I^- which prohibits the undesired halide segregation and facilitates the formation of perovskite crystals with enhanced thermal stability.[177] Rb^+ can greatly enhance the optoelectronic properties of the resultant perovskite when incorporated in small amounts due to the enlarged grain size of the perovskite films along with entropic gains and small internal energy input required for the formation of mixed perovskite concerning thermodynamics.[178]

Potassium (K^+) has been also applied to confer enhanced device performance in PSCs. K^+ addition can facilitate crystallization due to the decreased activation energy and enable the production of larger grain sizes leading to lower defect density at GBs, longer carrier lifetime and improved conductivity. K^+ incorporation in mixed cation perovskites was found to induce a small decrease to the bandgap value due to both occupation of A-site and/or interstitial ion in the lattice.[179] Generally, cation engineering represents one of the most effective approaches to tune the perovskite lattice and stabilize the photoactive black phase.

Halide optimization

The structure and optoelectronic properties of perovskites can alternatively be tuned through substitution in the halide anion X^- position. Modification of the halide anion changes the Pb-X bond length and accordingly the angle between X–Pb–X thus demonstrating one of the most effective approaches to tune the energy bandgap. Compounds with I^- show the smaller bandgap (in the range of 1.55–1.61 eV) whilst those with Cl^- have the highest bandgap (2.88–3.13 eV). The bandgap values perovskites with Br^- (2.0–2.44 eV) are between those with I^- and those with Cl^- whereas those of the mixed halide perovskites vary between those of the single halide ones.

Mixed-halide perovskites are ideal candidates for absorbers in photovoltaics because their optoelectronic properties can be effectively controlled by adjusting the halide concentration in the precursors.[180] However, upon illumination these mixed-halide perovskites undergo severe halide segregation resulting

to the formation of high bandgap Br-rich and low-bandgap I-rich domains, which act as carrier traps, inducing non-radiative electron-hole recombination.[181] As a result, significant voltage loss and reduced photostability is observed in PSCs based on mixed halide perovskites. The segregation of halide anions is generally initiated by halide defects in the perovskite structure, such as halide vacancies and interstitials, which provide low-energy migration pathways and cause the formation of iodide-rich and bromide-rich domains.[182,183] This defect-assisted halide migration has been proposed to be initiated by heat or light.[184] Once stored in the dark, entropically driven intermixing of halides returns the system to the initial homogeneous condition. Perovskite films with a low density of halide defects are more robust to halide migration and segregation phenomena.

Passivation approaches

Passivation of surface, grain boundaries (GB) and interface defects of perovskite films can be accomplished through the application of a wide variety of materials combined with different strategies and processes. Most of these passivation approaches include the use of organic small molecules, which exhibit tunable, optoelectronic properties and excellent stability and, therefore, they have been considered as efficient passivation agents.

Various organic donor-π-acceptor (D-π-A) small molecules with different electron density distributions were employed to efficiently passivate perovskite film defects.[185] Organic molecules, including functional groups, such as amino or carboxylate ones strongly coordinate with the under-coordinated Pb^{2+} especially when increasing electron density in the passivation moiety via employing nearby effective electron donor units.[186] Moreover, organic molecules with aromatic carboxylic acid groups also effectively coordinate with Pb^{2+} and passivate surface traps.[187] Upon controlling the –COOH content and optimising their concentration, the passivation effect of different defects can be rationalised.[188] Regarding amino functionalized molecules, their surface and GB defect passivation efficiency can be directly correlated to the alkyl chain length. An extended length of the alkyl chain in the amino bearing organic compounds results in multi-dimensional defect passivation and suppression of non-radiative charge carrier recombination.[189]

Hydrophobic organic small molecules incorporated at the fullerene/perovskite interface of inverted planar PSCs reduce the density of the surface and interfacial traps and offer increased long-term stability by inhibiting moisture penetration into the perovskite film.[190] Multi-functional molecular materials represent effective means to passivate defects, regulate film crystallinity and enhance crystal grain size.[300] Molecules featuring hydrophobic (hetero) aromatic cores and functionalized by ammonium or/and thiol groups not only ensure defect passivation of the A cation vacancy defects and unsaturated Pb^{2+} but also increase the perovskite crystal grain size and improve crystallinity. Fluorinated organic compounds simultaneously passivate surface defects, enlarge grain size, and induce surface hydrophobicity thus being beneficial for the device efficiency and stability.[191] In general, passivation of perovskite defects has been widely applied to successfully prolong both the device performance and stability under various internal and external factors.

Solvent engineering

Solvent engineering is also considered to be one of the most efficient approaches to control crystal growth and defect passivation in perovskite thin films.[192] This process relies on the evaporation of most of the perovskite solvent(s) but also leaves enough residual solvent in order to induce the formation of the chemical adducts with the perovskite precursors that determine the mechanism of nucleation, grain size evolution and crystallization. Some solvents used in this solvent engineering approach are diethyl ether (DEE), dichloromethane (DCM), N,N-dimethylformamide (DMF), dimethyl sulfoxide (DMSO). Isopropyl alcohol (IPA), acetone (ACE) and triethylenetetramine (TETA). The key strategies of solvent engineering can be categorized into the regulation of coordination ability of solvents

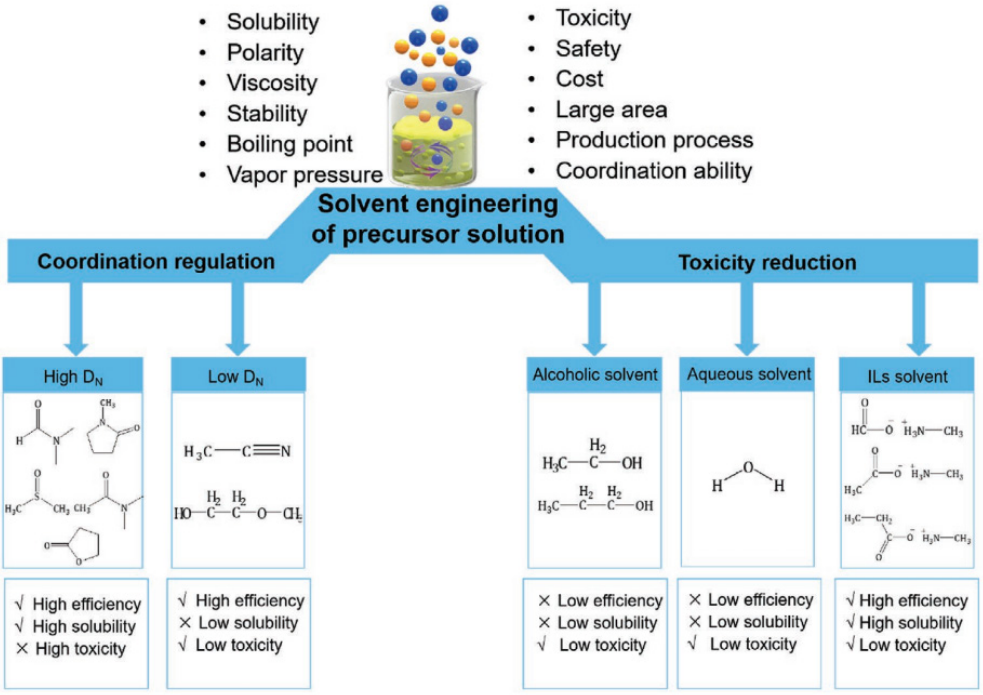

Fig. 8. Illustration of current development on solvent engineering of precursor solution in PSCs. Reproduced with permission from Ref. 193. Copyright 2021, John Wiley and Sons

by mixing solvents with high donor number (DN) with those with low DN and reducing the toxicity of precursor solution by using alcoholic, aqueous or ionic liquids (Ils)-based solvent) (Fig. 8).[193] This engineering approach starts with the application of the perovskite precursor onto the underlying charge transport layer, followed by the solvent engineering step that induces the formation of a highly compact, pinhole-free and smooth perovskite film with small surface roughness and full substrate coverage. Additionally, compositional engineering can also take place along with solvent engineering to enable optimal composition and optimized crystallization of the perovskite film and accordingly to improved solar cell performance.

Perovskite solar modules

Scaling up PSCs and producing efficient and stable modules is a prerequisite before this rapidly evolved technology enters into the market. During the last years, many research groups have developed deposition techniques to scale-up fabrication from small cells (with areas below 1 cm^2) to mini-modules with sizes ranging from 4 to 100 cm^2, and PCEs up to 21%.[194–197] It is evident that if PSC manufacturing can follow the pathways that have been developed for other thin-film solar cells, it will have serious potential for commercialization in the near future.

However, these modules suffer from environmental stability problems and their efficiency are severely affected by humidity and constant illumination. Particular attention is therefore paid to fabrication methods and passivation approaches that result in perovskite modules that are simple, low-cost and relatively stable. For example, carbon allotropes such as graphite, graphene, black carbon and carbon nanotubes, possessing low-cost, facile fabrication, high chemical stability and high conductivity, have been successfully applied as counter electrodes in mesoscopic modules.[198–200] Notably, a such mesoscopic module with an active area of 198 cm^2 and an efficiency of 6% is the largest perovskite module reported so far.[201] Planar perovskite modules also present exciting characteristics such as ease of fabrication and high efficiency which makes the two technologies comparable to each other.[202]

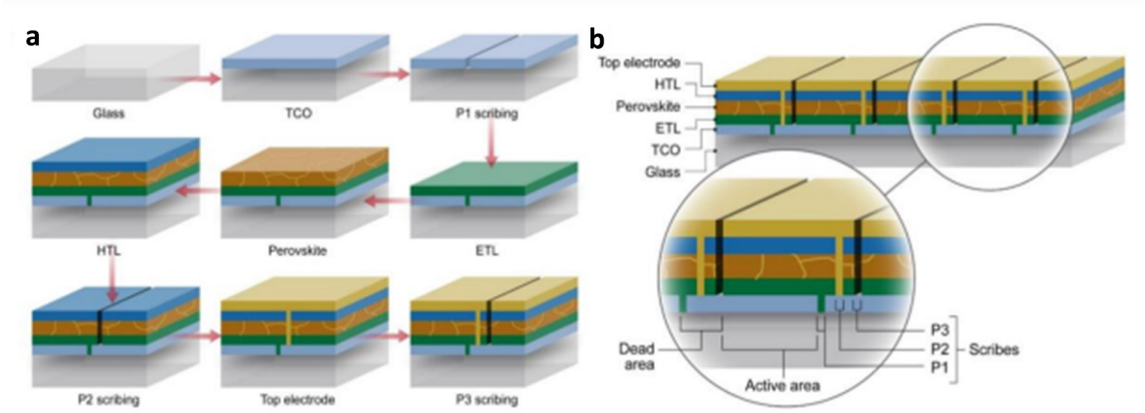

Fig. 9. Perovskite solar modules. (a) Manufacturing steps to make a module (step by step panels). A standard n-i-p perovskite device structure is used for illustration purpose. (b) Schematic of final module structure

In both these cases, module fabrication involves additional step compared to single-junction devices. In particular, it requires scribing steps (i.e., P1, P2 and P3 scribes), to divide a large-area device into sub-cells and form the electrical interconnections between sub-cells (Fig. 9 a). The P1 scribe is applied after coating the bottom electrode aiming to remove stripes of this electrode to pattern sub-cells. The P2 scribe is applied to the device layer stack just before the deposition of the top electrode. P2 scribe exposes the bottom electrode within the P2 scribe lines. The subsequent deposition of the top electrode connects the top electrode of one sub-cell to the bottom electrode of the next sub-cell (i.e., series connection). Finally, the P3 scribe isolates the top electrode between neighboring sub-cells to complete the monolithic interconnections (Fig. 9 b). The sub-cells interconnection in the module is critical for the device performance, and the carbon dioxide laser patterning technique as well as copper or aluminum grids have been proven highly suitable to successfully interconnect the sub-modules.[203]

The key design consideration for such module fabrication is to minimize the inactive area. Thus, it is important to minimize the fraction of the dead area (which is the area that does not contribute to the photogeneration of charge carriers) with respect to the total area that is the sum of the photoactive area and dead area, which is called the geometric fill factor (GFF). Several models and device designs have been considered leading to the module with a GFF of over 95%.[204] However, when increasing the module total area and GFF, a rapid decline in efficiency is commonly obtained. This indicates that further research efforts are still required to develop the large area but also efficient and stable perovskite modules as well as effective recycling protocols at the end of their life to secure a viable future for this rapidly evolved photovoltaic technology.[205]

Outlook and perspectives

Perovskite solar cells represent a rapidly advanced technology with an attractive figure of merits such as high efficiency, low material cost and short energy payback time. For further developments, however, significant advancements in efficiency stabilization should be made while novel materials and alternative large-area fabrication techniques should be developed. Besides their impressive attributes, perovskite solar cells still present issues regarding their stable operation under various stresses such as exposure to ambient and continuous illumination. To this end, the application of several compositional and dimensionality engineering approaches for the perovskite absorber combined with existing and novel passivation materials and approaches seem to be in the right direction. Moreover, judicious device engineering to address the interface induced degradation is a prerequisite to improve PSCs overall stability. Furthermore, the degradation of the perovskite absorber caused by environmental moisture or oxygen

can be successfully suppressed by suitable device encapsulation with materials and protocols borrowed by the more mature organic photovoltaic counterparts.

To realize their market entry, however, rapid advancements in the performance and stability of large-scale perovskite modules are urgently required. To this end, further improvements in the applied fabrication techniques and sophisticated design considerations that take into account the perovskite sub-cell structure, the sub-cells interconnection as well as the quality, recyclability and cost of used materials, including perovskites, interlayers, electrodes and substrate material, should be developed. Appropriate and reliable stability test protocols that researchers should subject their solar cells to are also needed in order for the literature results to be directly comparable. Up to now, scientific publications lack consistency in stability measurements adopted and this prevents the deeper understanding of degradation mechanisms that lead to the device failure. However, with the progress already make and rapid evolution of this technology, it is a common attribute that the remaining problems will be soon addressed thus facilitating immediate market entrance.

REFERENCES

[1] https://www.nrel.gov/pv/assets/pdfs/best-research-cell-efficiencies.20190802.pdf. (accessed 14/04/2020).

[2] **W. Shockley, H. J. Queisser,** J. Appl. Phys. 1961, 32, 510.

[3] **S. Rühle,** Sol. Energy, 2016, 130, 139.

[4] **A. Kojima, K. Teshima, Y. Shirai, T Miyasaka,** J. Amer. Chem. Soc., 2009, 131, 6050.

[5] **H.-S. Kim, C.-R. Lee, J.-H. Im, K.-B. Lee, T. Moehl, A. Marchioro, S.-J. Moon, R. Humphry-Baker, J.-H. Yum, J.E. Moser, M. Grätzel, N.-G. Park,** Sci. Rep., 2012, 2, 591.

[6] **M.M. Lee, J. Teuscher, T. Miyasaka, T.N. Murakami, H.J. Snaith,** Science 2012, 338, 643.

[7] **A. Fakharuddin, M. Vasilopoulou, A. Soultati, M.I. Haider, J. Briscoe, V. Fotopoulos, D. Di Girolamo, D. Davazoglou, A. Chroneos, A.R.b.M. Yusoff, A. Abate, L. Schmidt-Mende, M.K. Nazeeruddin,** Solar RRL, 2021, 5, 2000555.

[8] **A.R.b.M. Yusoff, M. Vasilopoulou, D.G. Georgiadou, L.C. Palilis, A. Abate, M.K. Nazeeruddin,** Energy Environ. Sci., 2021, 14, 2906.

[9] **C. Igci, H. Kanda, S.-M. Yoo, A.A. Sutanto, O.A. Syzgantseva, M.A. Syzgantseva, V. Jankauskas, K. Rakstys, M. Mensi, H. Kim, A.M. Asiri, M.K. Nazeeruddin,** Solar RRL, 2021, 2100667. https://doi.org/10.1002/solr.202100667

[10] **J. Urieta-Mora, I. García-Benito, L.A. Illicachi, J. Calbo, J. Aragó, A. Molina-Ontoria, E. Ortí, N. Martín, M.K. Nazeeruddin,** Solar RRL, 2021, 5, 2100650.

[11] **L. Huang, Z. Xing, X. Tang, D. Li, X. Meng, X. Hu, T. Hu, Y. Chen,** J. Mater. Chem A, 2021, 9, 16178.

[12] **S. Yang, Q. Han, L. Wang, Y. Zhou, F. Yu, C. Li, X. Cai, L. Gao, C. Zhang, T. Ma,** Chem. Eng. J., 2021, 426, 131838.

[13] **H. Bi, B. Liu, D. He, L. Bai, W. Wang, Z. Zang, J. Chen,** Chem. Eng. J., 2021, 418, 129375.

[14] **P. Song, L. Shen, L. Zheng, K. Liu, W. Tian, J. Chen, Y. Luo, C. Tian, L. Xie, Z. Wei,** Nano Sel., 2021, 2, 1779.

[15] **Y. Du, J. Wu, X. Zhang, Q. Zhu, M. Zhang, X. Liu, Y. Zou, S. Wang, W. Sun,** J. Energy Chem., 2021, 52, 84.

[16] **J. Burschka, N. Pellet, S.-J. Moon, R. Humphry-Baker, P. Gao, M.K. Nazeeruddin, M. Grätzel,** Nature 2013, 499, 316.

[17] **M. Liu, M.B. Johnston, H.J. Snaith,** Nature, 2013, 501, 395.

[18] **E.H. Jung, N.J. Jeon, E.Y. Park, C.S. Moon, T.J. Shin, T.-Y. Yang, J.H. Noh, J. Seo,** Nature, 2019, 567, 511.

[19] **M.O. Reese, S.A. Gevorgyan, M. Jørgensen, E. Bundgaard, S.R. Kurtz, D.S. Ginley, D.C. Olson, M.T. Lloyd, P. Morvillo, E.A. Katz, A. Elschner,** Sol. Energy Mater. Sol. Cells, 2011, 95, 1253.

[20] **X. Yang, X. Yan, W. Wang, X. Zhu, H. Li, W.C. Ma,** Org. Electron., 2016, 34, 79.

[21] **Y. Liu, C. Xie, W. Tan, X. Liu, Y. Yuan, Q. Xie, Y. Li, Y. Gao,** Org. Electron., 2019, 71, 123.

[22] **N. Rolston, K.A. Bush, A.D. Printz, A. Gold-Parker, Y. Ding, M.F. Toney,** Adv. Energy Mater., 2018, 8, 1802139.

[23] **P. Calado, A.M. Telford, D. Bryant, X. Li, J. Nelson, B.C. O'Regan, P.R.F. Barnes,** Nat. Commun., 2016, 7, 13831.

[24] **J.M. Frost, K.T. Butler, F. Brivio, C.H. Hendon, M. van Schilfgaarde, A. Walsh,** Nano Lett., 2014 , 14, 2584 .

[25] **L. Schmidt-Mende, V. Dyakonov, S. Olthof, F. Ünlü, K.M. Trong Lê, S. Mathur, A.D. Karabanov, D.C. Lupascu, L.M Herz, A. Hinderhofer, F. Schreiber, A. Chernikov, D.A. Egger, O. Shargaieva, C. Cocchi, E. Unger, M. Saliba, M.M. Byranvand, M. Kroll, F. Nehm, K. Leo, A. Redinger, J. Höcker, T. Kirchartz, J. Warby, E. Gutierrez-Partida, D. Neher, M. Stolterfoht, U. Würfel, M. Unmüssig, J. Herterich, C. Baretzky, J. Mohanraj, M. Thelakkat, C. Maheu, W. Jaegermann, T. Mayer, J. Rieger, T. Fauster, D. Niesner, F. Yang, S. Albrecht, T. Riedl, A. Fakharuddin, M. Vasilopoulou, Y. Vaynzof, D. Moia, J. Maier, M. Franckevičius, V. Gulbinas, R.A. Kerner, L. Zhao, B.P. Rand, N. Glück, T. Bein, F. Matteocci, L.A. Castriotta, A. Di Carlo, M. Scheffler, C. Draxl,** APL Materials, 2021, 9, 109202.

[26] **H.S. Kim, C.R. Lee, J.H. Im, K.B. Lee, T. Moehl, A. Marchioro, S.J. Moon, R. Humphry-Baker, J.H. Yum, J.E. Moser, M. Grätzel, N.G. Park,** Sci. Rep., 2012, 2, 591.

[27] **T. Duong, H. Pham, T.C. Kho, P. Phang, K.C. Fong, D. Yan, Y. Yin, J. Peng, M.A. Mahmud, S. Gharibzadeh, B.A. Nejand, I.M. Hossain, M.R. Khan, N. Mozaffari, Y. Wu, H. Shen, J. Zheng, H. Mai, W. Liang, C. Samundsett, M. Stocks, K. McIntosh, G.G. Andersson, U. Lemmer, B.S. Richards, U.W. Paetzold, A. Ho-Baillie, Y. Liu, D. Macdonald, A. Blakers, J. Wong-Leung, T. White, K. Weber, K. Catchpole,** Adv. Energy Mater., 2020, 10, 1903553.

[28] **A. Krishna, A.C. Grimsdale,** J. Mater. Chem. A, 2017, 5, 16446.

[29] **C. Yang, X. Shan, T. Xie,** Photonics, 2020, 7, 47.

[30] **S. De Wolf, J. Holovsky, S.J. Moon, P. Löper, B. Niesen, M. Ledinsky, F.J. Haug, J.H. Yum, C. Ballif,** J. Phys. Chem. Lett., 2014, 5, 1035.

[31] **W. Chen, Y. Zhou, G. Chen, Y. Wu, B. Tu, F.-Z. Liu, L. Huang, A.M.C. Ng, A.B. Djurišić, Z. He,** Adv. Energy Mater., 2019, 9, 1803872.

[32] **S. Collavini, S.F. Völker, J.L. Delgado,** Angew. Chem. Int. Ed., 2015, 54, 9757.

[33] **A. Mei, X. Li, L. Liu, Z. Ku, T. Liu, Y. Rong, M. Xu, M. Hu, J. Chen, Y. Yang, M. Grätzel, H. Han,** Science, 2014, 345, 295.

[34] **Q. Wang, W. Zhang, Z. Zhang, S. Liu, J. Wu, Y. Guan, A. Mei, Y. Rong, Y. Hu, H. Han,** Adv. Energy Mater. 2020, 10, 1903092.

[35] **J.H. Im, C.R. Lee, J.W. Lee, S.W. Park, N.G.** Park, Nanoscale, 2011, 3, 4088.

[36] **P. Lopez-Varo, J.A. Jiménez-Tejada, M. García-Rosell, S. Ravishankar, G. Garcia-Belmonte, J. Bisquert, O. Almora,** Adv. Energy Mater., 2018, 8, 1702772.

[37] **D. Yang, R. Yang, K. Wang, C. Wu, X. Zhu, J. Feng, X. Ren, G. Fang, S. Priya, S. (Frank) Liu,** Nat. Commun., 2018, 9, 3239.

[38] **P. Docampo, J.M. Ball, M. Darwich, G.E. Eperon, H.J. Snaith,** Nat. Commun., 2013, 4, 2761.

[39] **J. Tang, D. Jiao, L. Zhang, X. Zhang, X. Xu, C. Yao, J. Wu, Z. Lan,** Sol. Energy, 2018, 161, 100.

[40] **G.E. Eperon, S.D. Stranks, C. Menelaou, M.B. Johnston, L.M. Herz, H. J. Snaith,** Energy Environ. Sci., 2014, 7, 982.

[41] **W.E.I. Sha, X. Ren, L. Chen, W.C.H. Choy,** Appl. Phys. Lett., 2015, 106, 221104.

[42] **S.N. Habisreutinger, T. Leijtens, G.E. Eperon, S.D. Stranks, R.J. Nicholas, H.J. Snaith,** Nano Lett., 2014, 14, 5561.

[43] **H. Zhou, Y. Shi, Q. Dong, H. Zhang, Y. Xing, K. Wang, Y. Du, T. Ma,** J. Phys. Chem. Lett., 2014, 5, 3241.

[44] **H. Han, U. Bach, Y.-B. Cheng, R. A. Caruso, C. MacRae,** Appl. Phys. Lett., 2009, 94, 103102.

[45] **Q. He, K. Yao, X. Wang, X. Xia, S. Leng, F. Li,** ACS Appl. Mater. Interfaces, 2017, 9, 41887.

[46] **C.C. Stoumpos, M.G. Kanatzidis,** Acc. Chem. Res., 2015, 48, 2791.

[47] **X. Zhang, J.-X. Shen, C.G. Van de Walle,** Adv. Energy Mater., 2020, 10, 1902830.

[48] **G. Kieslich, S. Sun, A.K. Cheetham,** Chem. Sci., 2014, 5, 4712.

[49] **M.I. Hossain, F.H. Alharbi, N. Tabet,** Sol. Energy, 2015, 120, 370.

[50] **C. Zuo, L. Ding,** Small, 2015, 11, 5528.

[51] **S. Chatterjee, A.J. Pal,** J. Phys. Chem. C, 2016, 120, 1428.

[52] **B. Conings, J. Drijkoningen, N. Gauquelin, A. Babayigit, J. D'Haen, L. D'Olieslaeger, A. Ethirajan, J. Verbeeck, J. Manca, E. Mosconi, F.D. Angelis, H.-G. Boyen,** Adv. Energy Mater., 2015, 5, 1500477.

[53] **M.T. Horantner, T. Leijtens, M.E. Ziffer, G.E. Eperon, M.G. Christoforo, M.D. McGehee, H.J. Snaith,** ACS Energy Lett., 2017, 2, 2506.

[54] **B.A. Nejand, V. Ahmadi, S. Gharibzadeh, H.R. Shahverdi,** ChemSusChem, 2016, 9, 302.

[55] **Y. Guo, H. Lei, L. Xiong, B. Li, G. Fang,** J. Mater. Chem. A, 2018, 6, 2157.

[56] **N.J. Jeon, J.H. Noh, Y.C. Kim, W.S. Yang, S. Ryu, S.I. Seok,** Nat. Mater., 2014, 13, 897.

[57] **N.J. Jeon, J.H. Noh, W.S. Yang, Y.C. Kim, S. Ryu, J. Seo, S.I. Seok,** Nature, 2015, 517, 476.

[58] **M. Saliba, T. Matsui, J.-Y. Seo, K. Domanski, J.-P. Correa-Baena, M.K. Nazeeruddin, S.M. Zakeeruddin, W. Tress, A. Abate, A. Hagfeldt, M. Grätzel,** Energy Environ. Sci., 2016, 9, 1989.

[59] **M. Saliba, T. Matsui, K. Domanski, J.-Y. Seo, A. Ummadisingu, S.M. Zakeeruddin, J.-P. Correa-Baena, W.R. Tress, A. Abate, A. Hagfeldt, M. Grätzel,** Science, 2016, 354, 206.

[60] **J.V. Patil, S.S. Mali, C.K. Hong,** Solar RRL, 2020, 4, 2000164.

[61] **C. Lan, Z. Zhou, R. Wei, J.C. Ho,** Mater. Today Energy, 2019, 11, 61.

[62] **Y. Zheng, T. Niu, X. Ran, J. Qiu, B. Li, Y. Xia, Y. Chen, W. Huang,** J. Mater. Chem. A, 2019, 7, 13860.

[63] **J. Yan, W. Qiu, G. Wu, P. Heremans, H. Chen,** J. Mater. Chem. A, 2018, 6, 11063.

[64] **T.H. Chowdhury, M. Akhtaruzzaman, M.E. Kayesh, R. Kaneko, T. Noda, J.-J. Lee, A. Islam,** Sol. Energy, 2018, 171, 652.

[65] **G.E. Eperon, G.M. Paterno, R.J. Sutton, A. Zampetti, A.A. Haghighirad, F. Cacialli, H.J. Snaith,** J. Mater. Chem. A, 2015, 3, 19688.

[66] **I.C. Smith, E.T. Hoke, D. Solis-Ibarra, M.D. McGehee, H.I. Karunadasa,** Angew. Chem. Int. Ed., 2014, 53, 11232.

[67] **J.C. Blancon, H. Tsai, W. Nie, C.C. Stoumpos, L. Pedesseau, C. Katan, M. Kepenekian, C.M. Soe, K. Appavoo, M.Y. Sfeir, S. Tretiak, P.M. Ajayan, M.G. Kanatzidis, J. Even, J.J. Crochet, A.D. Mohite,** Science, 2017, 355, 1288.

[68] **C.C. Stoumpos, D.H. Cao, D.J. Clark, J. Young, J.M. Rondinelli, J.I. Jang, J.T. Hupp, M.G. Kanatzidis,** Chem. Mater., 2016, 28, 2852.

[69] **T. Ishihara, J. Lumin,** 1994, 60, 269.

[70] **Y. Yang, D.P. Ostrowski, R.M. France, K. Zhu, J. Van De Lagemaat, J.M. Luther, M.C. Beard,** Nat. Photonics, 2016, 10, 53.

[71] **M. Hirasawa, T. Ishihara, T. Goto, K. Uchida, N. Miura,** Phys. B, 1994, 201, 427.

[72] **X. Hong, T. Ishihara, A. Nurmikko,** Phys. Rev. B, 1992, 45, 6961.

[73] **J. Cho, Y.H. Choi, T.E. O'Loughlin, L. De Jesus, S. Banerjee,** Chem. Mater., 2016, 28, 6909.

[74] **T. Zhang, M.I. Dar, G. Li, F. Xu, N. Guo, M. Gratzel, Y. Zhao,** Sci. Adv., 2017, 3, e1700841.

[75] **L.N. Quan, M. Yuan, R. Comin, O. Voznyy, E.M. Beauregard, S. Hoogland, A. Buin, A.R. Kirmani, K. Zhao, A. Amassian, D.H. Kim, E.H. Sargent,** J. Am. Chem. Soc., 2016, 138, 2649.

[76] **J. Liu, J. Leng, K. Wu, J. Zhang, S. Jin,** J. Am. Chem. Soc., 2017, 139, 1432.

[77] **B.-E. Cohen, M. Wierzbowska, L. Etgar,** Adv. Funct. Mater., 2017, 27, 1604733.

[78] **Z. Wang, Q. Lin, F. P. Chmiel, N. Sakai, L. M. Herz, H. J. Snaith,** Nat. Energy, 2017, 6, 17135.

[79] **N. Li, Z. Zhu, C.-C. Chueh, H. Liu, B. Peng, A. Petrone, X. Li, L. Wang, A.K.Y. Jen,** Adv. Energy Mater., 2017, 7, 1601307.

[80] **G. Grancini, C. Roldán-Carmona, I. Zimmermann, E. Mosconi, X. Lee, D. Martineau, S. Narbey, F. Oswald, F. De Angelis, M. Graetzel, M.K. Nazeeruddin,** Nat. Commun. 2017, 1, 8, 15684.

[81] **K.H. Wong, K. Ananthanarayanan, M.D. Heinemann, J. Luther, P. Balaya,** Sol. Energy, 2012, 86, 3190.

[82] **W. Chen, Y. Zhou, L. Wang, Y. Wu, B. Tu, B. Yu, F. Liu, H.-W. Tam, G. Wang, A. B. Djurišić, L. Huang, Z. He,** Adv. Mater., 2018, 30, 1800515.

[83] **N. Chaudhary, R. Chaudhary, J.P. Kesari, A. Patra, S. Chand,** J. Mater. Chem. C, 2015, 3, 11886.

[84] **G. Terán-Escobar, J. Pampel, J.M. Caicedo, M. Lira-Cantú,** Energy Environ. Sci., 2013, 6, 3088.

[85] **B.-W. Park, N. Kedem, M. Kulbak, D.Y. Lee, W.S. Yang, N.J. Jeon, J. Seo, G. Kim, K.J. Kim, T.J. Shin, G. Hodes, D. Cahen, S.I. Seok,** Nat. Commun., 2018, 9, 3301.

[86] **V.K. LaMer, R.H. Dinegar,** J. Am. Chem. Soc., 1950, 72, 4847.

[87] **W. Zhai, J. Lin, Q. Li, K. Zheng, Y. Huang, Y. Yao, X. He, L. Li, C. Yu, C. Liu, Y. Fang, Z. Liu, C. Tang,** Chem. Mater., 2018, 30, 3714.

[88] **Y. Kesari, A. Athaale,** Mater. Lett., 2015, 159, 87.

[89] **J. Jancik, A.J. Prochazkova, M.C. Scharber, A. Kovalenko, J. Masilko, N.S. Sariciftci, M. Weiter, J. Krajcovic,** Cryst. Growth Des., 2020, 20, 1388.

[90] **A. Abate, F. Giordano, J.C. Baena, J. Decoppet,** Sci. Adv., 2016, 2, e1501170.

[91] **W.S. Yang, J.H. Noh, N.J. Jeon, Y.C. Kim, S. Ryu, J. Seo, S. I. Seok,** Science, 2015, 348, 1234.

[92] **J.W. Lee, T.Y. Lee, P.J. Yoo, M. Grätzel, S. Mhaisalkar, N.G. Park,** J. Mater. Chem. A, 2014, 2, 9251.

[93] **M. Yang, R. Guo, K. Kadel, Y. Liu, K. O'Shea, R. Bone, X. Wang, J. He, W. Li,** J. Mater. Chem. A, 2014, 2, 19616.

[94] **X. Hou, J. Zhou, S. Huang, W. Ou-Yang, L. Pan, X. Chen,** Chem. Eng. J., 2017, 330, 947.

[95] **P. Tonui, S.O. Oseni, G. Sharma, Q. Yan, G.T. Mola,** Renewable Sustainable Energy Rev., 2018, 91, 1025.

[96] **K.L. Gardner, J.G. Tait, T. Merckx, W. Qiu, U.W. Paetzold, L. Kootstra, M. Jaysankar, R. Gehlhaar, D. Cheyns, P. Heremans, J. Poortmans,** Adv. Energy Mater., 2016, 6, 1600386.

[97] **K. Liao, C. Li, L. Xie, Y. Yuan, S. Wang, Z. Cao, L. Ding, F. Hao,** Nano-Micro Lett., 2020, 12, 156.

[98] **Z. Yang, S. Zhang, L. Li, W. Chen,** J. Materiomics, 2017, 3, 231.

[99] **S.D. Stranks, P.K. Nayak, W. Zhang, T. Stergiopoulos, H.J. Snaith,** Angew. Chem., Int. Ed., 2015, 54, 3240.

[100] **T.-B. Song, Q. Chen, H. Zhou, C. Jiang, H.-H. Wang, Y. (M.) Yang, Y. Liu, J. You, Y. Yang,** J. Mater. Chem. A., 2015, 3, 9032.

[101] **H. Zhou, Q. Chen, Y. Yang,** MRS Bull., 2015, 40, 667.

[102] **Q. Chen, H. Zhou, Z. Hong, S. Luo, H.-S. Duan, H.-H. Wang, Y. Liu, G. Li, Y. Yang,** J. Am. Chem. Soc., 2014, 136, 622.

[103] **M. Prakasam, O. Viraphong, O. Cambon, A. Largeteau,** Chapter 15 – Hydrothermal Crystal Growth and Applications, in: N.P. Bansal, M. Kusnezoff, K. Shimamura (Eds.), Advances in Solid Oxide Fuel Cells and Electronic Ceramics, John Wiley & Sons, Inc., 2015, pp.151–156.

[104] **S.-H. Feng, G.-H. Li,** Chapter 4 – Hydrothermal and Solvothermal Syntheses, in: R. Xu, Y. Xu (Eds.), Modern Inorganic Synthetic Chemistry, Elsevier B.V., 2017, pp. 73–104.

[105] **R.A. Laudise,** Chem. Eng. News, 1987, 65, 30.

[106] **C.S. Cundy, P.A. Cox,** Chem. Rev., 2003, 103, 663.

[107] **C.R. Kagan, D.B. Mitzi, C.D. Dimitrakopoulos,** Science, 1999, 286, 945.

[108] **A. Kojima, K. Teshima, Y. Shirai, T. Miyasaka,** J. Am. Chem. Soc., 2009, 131, 6050.

[109] **Q. Cao, S. Yang, Q. Gao, L. Lei, Y. Yu, J. Shao, Y. Liu,** ACS Appl. Mater. Interfaces, 2016, 8, 7854.

[110] **Z. Li, P. Li, G. Chen, Y. Cheng, X. Pi, X. Yu, D. Yang, L. Han, Y. Zhang, Y. Song,** ACS Appl. Mater. Interfaces, 2020, 12, 39082.

[111] **C. Quinto, A. Linares, E. Llarena, C. Montes, O. González, D. Molina, A. Pío, L. Ocaña, M. Friend, M. Cendagorta,** Screen Printing for Perovskite Solar Cells Metallization, 31st European Photovoltaic Solar Energy Conference and Exhibition, 2015, pp. 1144–1148.

[112] **Y.Y. Kim, T.-Y. Yang, R. Suhonen, A. Kemppainen, K. Hwang, N.J. Jeon,** Nat. Commun., 2020, 11, 5146.

[113] **Y. Wang, C. Duan, P. Lv, Z. Ku, J. Lu, F. Huang, Y.-B. Cheng,** Natl. Sci. Rev., 2021, 8, nwab075.

[114] **A. Kogo, Y. Sanehira, M. Ikegami, T. Miyasaka,** J. Mater. Chem. A, 2015, 3, 20952–20957.

[115] **W.-Q. Wu, F. Huang, D. Chen, Y.-B. Cheng, R.A. Caruso,** Adv. Funct. Mater., 2015, 25, 3264–3272.

[116] **P. Qin, A.L. Domanski, A.K. Chandiran, R. Berger, H.-J. Butt, M.I. Dar, T. Moehl, N. Tetreault, P. Gao, S. Ahmad, M.K. Nazeeruddin, M. Grätzel,** Nanoscale, 2014, 6, 1508–1514.

[117] **J.T.W. Wang, J.M. Ball, E.M. Barea, A. Abate, J.A. Alexander-Webber, J. Huang, M. Saliba, I.M. Sero, J. Bisquert, H.J. Snaith, R.J. Nicholas,** Nano Lett., 2014, 14, 724–730.

[118] **A.K. Chandiran, A. Yella, M.T. Mayer, P. Gao, M.K. Nazeeruddin, M. Grätzel,** Adv. Mater., 2014, 26, 4309–4312.

[119] **G.S. Han, H.S. Chung, B.J. Kim, D.H. Kim, J.W. Lee, B.S. Swain, K. Mahmood, J.S. Yoo, N.G. Park, J.H. Lee, H.S. Jung,** J. Mater. Chem. A, 2015, 3, 9160–9164.

[120] **Y. Ogomi, K. Kukihara, S. Qing, T. Toyoda, K. Yoshino, S. Pandey, H. Momose, S. Hayase,** ChemPhysChem, 2014, 15, 1062–1069.

[121] **M. Ebrahimi, A. Kermanpur, M. Atapour, S. Adhami, R.H. Heidari, E. Khorshibi, N. Irannejad, B. Rezaie,** Sol. Energy Mater. Sol. Cells, 2020, 208, 110407.

[122] **S.S. Mali, C.S. Shim, H.K. Park, J. Heo, P.S. Patil, C.K. Hing,** Chem. Mater., 2015, 27, 1541–1551.

[123] **A.K. Chandiran, A. Yella, M.T. Mayer, P. Gao, M.K. Nazeeruddin, M. Grätzel,** Adv. Mater., 2014, 26, 4309–4312.

[124] **H. Dong, X. Guo, W. Li, L. Wang,** RSC Adv., 2014, 4, 60131–60134.

[125] **H.M.A. Javed, M.I. Ahmad, W. Que, A.A. Qureshi, M. Sarfaraz, S. Hussain, M.Z. Iqbal, M. Zubair, N.M. Shahid, T.S. Al Garni,** Surfaces and Interfaces, 2021, 23, 101033.

[126] **G.S. Han, H.S. Chung, B.J. Kim, D.H. Kim, J.W. Lee, B.S. Swain, K. Mahmood, J.S. Yoo, N.G. Park, J.H. Lee, H.S. Jung,** J. Mater. Chem. A, 2015, 3, 9160–9164.

[127] **Z. Zhu, J. Ma, Z. Wang, C. Mu, Z. Fan, L. Du, Y. Bai, L. Fan, H. Yan, D.L. Phillips, S. Yang,** J. Am. Chem. Soc., 2014, 136, 3760–3763.

[128] **R.D. Chavan, M.M. Tavakoli, D. Prochowicz, P. Yadav, S.S. Lote, S.P. Bhoite, A. Nimbalkar, C.K. Hong,** ACS Appl. Mater. Interfaces, 2020, 12, 7, 8098–8106.

[129] **J. Dong, Y. Zhao, H. Wei, J. Xiao, X. Xu, J. Luo, J. Xu, D. Li, Y. Luo, Q. Meng,** Chem. Commun., 2014, 50, 13381–13384.

[130] **K. Mahmood, B.S. Swain, A. Amassian,** Nanoscale, 2015, 7, 12812–12819.

[131] **X. Zhao, H. Shen, R. Sun, Q. Luo, X. Li, Y. Zhou, M. Tai, J. Li, Y. Gao, X. Li, H. Lin,** Sol. RRL, 2018, 1700194.

[132] **K. Mahmood, B.S. Swain, A. Amassian,** Adv. Energy Mater., 2015, 5, 1500568.

[133] **S. Li, P. Zhang, H. Chen, Y. Wang, D. Liu, J. Wu, H. Sarvari, Z.D. Chen,** J. Power Sources, 2017, 342, 990–997.

[134] **Q. Liu, M.-C. Qin, W.-J. Ke, X.L. Zheng, Z. Chen, P.-L. Qin, L.B. Xiong, H.W. Lei, J.-W. Wan, J. Wen, G. Yang, J.-J. Ma, Z.-Y. Zhang, G.-J. Fang,** Adv. Funct. Mater., 2016, 26, 6069–6075.

[135] **B. Roose, J.-P.C. Baena, K.C. Gödel, M. Graetzel, A. Hagfeldt, U. Steiner, A. Abate,** Nano Energy, 2016, 30, 517–522.

[136] **B. Roose, C.M. Johansen, K. Dupraz, T. Jaouen, P. Aebi, U. Steiner, A. Abate,** J. Mater. Chem. A, 2018, 6, 1850.

[137] **Q. Guo, J. Wu, Y. Yang, X. Liu, Z. Lan, J. Lin, M. Huang, Y. Wei, J. Dong, J. Jia, Y. Huang,** Research, 2019, 2019, 4049793.

[138] **Q. Wang, C. Peng, L. Du, H. Li, W. Zhang, J. Xie, H. Qi, Y. Li, L. Tian, Y. Huang,** Adv. Mater. Interfaces, 2020, 7, 1901866.

[139] **J. Song, G. Li, D. Wang, W. Sun, J. Wu, Z. Lan,** Sol. RRL, 2020, 4, 1900558.

[140] **K.-H. Jung, J.-Y. Seo, S. Lee, H. Shin, N.-G. Park,** J. Mater. Chem. A, 2017, 5, 24790–24803.

[141] **E. Aydin, M. De Bastiani, S. De Wolf,** Adv. Mater., 2019, 31, e1900428.

[142] **K. Wang, S. Olthof, W.S. Subhani, X. Jiang, Y. Cao, L. Duan, H. Wang, M. Du, S. (Frank) Liu,** Nano Energy, 2020, 68, 104289.

[143] **M. Zheng, W. Xu, H.C. Yuan, J. Wu,** J. Alloys Compd., 2020, 823, 153730.

[144] **N. Aristidou, I. Sanchez-Molina, T. Chotchuangchutchaval, M. Brown, L. Martinez, T. Rath, S.A. Haque,** Angew. Chemie. Int. Ed., 2015, 54, 8208–8212.

[145] **L. Calil, S. Kazim, M. Gratzel, S. Ahmad,** Angewandte Chemie, 2016, 55, 14522–14545.

[146] **H.S. Kim, C.-R. Lee, J.-H. Im, K.-B. Lee, T. Moehl, A. Marchioro, S.J. Moon, R. Humphry-Baker, J.-H. Yum, J.E. Moser, M. Grätzel, N.-G. Park,** Sci. Rep., 2012, 1–7.

[147] **H.J. Snaith, M. Grätzel,** Appl. Phys. Lett., 2006, 89, 262114.

[148] **M.M. Tavakoli, W. Tress, J.V. Milić, D. Kubicki, L. Emsley, M. Grätzel,** Energy Environ. Sci., 2018, 11, 3310–3320.

[149] **M. Saliba, T. Matsui, J.Y. Seo, K. Domanski, J.-P. Correa-Baena, M.K. Nazeeruddin, S.M. Zakeeruddin, W. Tress, A. Abate, A. Hagfeldt, M. Grätzel,** Energy Environ. Sci., 2016, 9, 1989–1997.

[150] **N.J. Jeon, H.G. Lee, Y.C. Kim, J. Seo, J.H. Noh, J. Lee, S.I. Seok,** J. Am. Chem. Soc., 2014, 136, 22, 7837–7840.

[151] **J.H. Heo, S.H. Im, J.H. Noh, T.N. Mandal, C.-S. Lim, J.A. Chang, Y.H. Lee, H.J. kim, A. Sarkar, M.K. Nazeeruddin, M. Grätzel, S.I. Seok,** Nat. Photonics, 2013, 7, 486–491.

[152] **W.S. Yang, J.H. Noh, N.J. Jeon, Y.C. kim, S. Ryu, J. Seo, S.I. Seok,** Science, 2015, 348, 1234–1237.

[153] **R. Ranjan, B, Usmani, S. Ranjan, H.C. Weerasinghe, A. Singh, A. Garg, R.K. Gupta,** Sol. Energy Mater. Sol. Cells, 2019, 202, 110130.

[154] **R.D. Chavan, P. Yadav, M.M. Tavakoli, D. Prochowicz, A. Nimbalkar, S.P. Bhoite, P.N. Bhosale, C.K. Hong,** Sustainable Energy Fuels, 2020, 4, 843.

[155] **P. Qin, N. Tetreault, M.I. Dar, P. Gao, K.L. McCall, S.R. Rutter, S.D. Ogier, N.D. Forrest, J.S. Bissett, M.J. Simms, A.J. Page, R. Fisher, M. Grätzel, M.K. Nazeeruddin,** Adv. Energy Mater., 2014, 5, 1400980.

[156] **K. Do, H. Choi, K. Lim, H. Jo, J.W. Cho, M.K. Nazeeruddin, J. Ko,** Chem. Commun., 2014, 50, 10971–10974.

[157] **K. Rakstys, A. Abate, M.I. Dar, P. Gao, V. Jankauskas, G. Jacopin, E. Kamarauskas, S. Kazim, S. Ahmad, M. Grätzel, M.K. Nazeeruddin,** J. Am. Chem. Soc., 2015, 137, 51, 16172–16178.

[158] **X. Liu, X. Ding, Y. Ren, Y. Yang, Y. Ding, X. Liu, A. Alsaedi, T. Hayat, J. Yao, S. Dai,** J. Mater. Chem. C, 2018, 6, 12912–12918.

[159] **F. Zhang, X. yang, M. Cheng, W. Wang, L. Sun,** Nano Energy, 2016, 20, 108–116.

[160] **Y.H. Chiang, H.-H. Chou, W.-T. Cheng, Y.-R. Li, C.-Y. Yeh, P. Chen,** ACS Energy Lett., 2018, 3, 7, 1620–1626.

[161] **G. Li, K. Deng, Y. Dou, Y. Liao, D. Wang, J. Wu, Z. Lan,** Solar Energy, 2019, 193, 111–117.

[162] **A. Baskir, S. Shukla, R. Bashir, R. Patidar, A. Bruno, D. Gupta, M.S. Satti, Z. Akhter,** Solar Energy, 2020, 196, 367–378.

[163] **A. Fakharuddin, M. Vasilopoulou, A. Soultati, M.I. Haider, J. Briscoe,V. Fotopoulos, D. Di Girolamo, D. Davazoglou, A. Chroneos, A.R.b.M. Yusoff, A. Abate, L. Schmidt-Mende, M.K. Nazeeruddin,** Solar RRL, 2021, 5, 2000555.

[164] **J.-W. Lee, D.-J. Seo, A.-N. Cho, N.-G. Park,** Adv. Mater., 2014, 26, 4991.

[165] **M.A. Haque, A.D. Sheikh, X. Guan, T. Wu,** Adv. Energy Mater., 2017, 7, 1602803.

[166] **N. Timasi, S. Tafazoli, E. Nouri, M.R. Mohammadi, Y. Li,** Photochem. Photobiol. Sci., 2019, 18, 1228.

[167] **L. Zuo, S. Dong, N. De Marco, Y. Hsieh, S. Bae,** J. Am. Chem. Soc., 2016, 138, 15710.

[168] **X. Fang, Y. Wu, Y. Lu, Y. Sun, S. Zhang, J. Zhang, W. Zhang, N. Yuan, J. Ding,** J. Mater. Chem. C, 2017, 5, 842.

[169] **X. Fang, Y. Wu, Y. Lu, Y. Sun, S. Zhang, J. Zhang, W. Zhang, N. Yuan, J. Ding,** J. Mater. Chem. C, 2017, 5, 842.

[170] **J. Liu, C. Gao, X. He, Q. Ye, L. Ouyang, D. Zhuang, C. Liao, J. Mei, W. Lau,** ACS Appl. Mater. Interfaces, 2015, 7, 24008

[171] **J.-W. Lee, D.-H. Kim, H.-S. Kim, S.-W. Seo, S.M. Cho, N.-G. Park,** Adv. Energy Mater., 2015, 5, 1501310.

[172] **M. Johnson, S.V. Baryshev, E. Thimsen, M. Manno, X. Zhang, I.V. Veryovkin, C. Leighton, E.S. Aydil,** Energy Environ. Sci., 2014, 7, 1931.

[173] **J. Cao, S.X. Tao, P.A. Bobbert, C.-P. Wong, N. Zhao,** Adv. Mater., 2018, 30, 1707350.

[174] **Y. Wang, T. Zhang, M. Kan, Y. Zhao,** J. Am. Chem. Soc., 2018, 140, 12345.

[175] **D.M. Trots, S.V. Myagkota,** J. Phys. Chem. Solids, 2008, 69, 2520.

[176] **P. Yadav, M.I. Dar, N. Arora, E.A. Alharbi, F. Giordano, S.M. Zakeeruddin, M. Grätzel,** Adv. Mater., 2017, 29, 1701077.

[177] **C. Yi, J. Luo, S. Meloni, A. Boziki, N. Ashari-Astani, C. Grätzel, S.M. Zakeeruddin, U. Röthlisberger, M. Grätzel,** Energy Environ. Sci., 2016, 9, 656.

[178] **J.K. Nam, S.U. Chai, W. Cha, Y.J. Choi, W. Kim, M.S. Jung, J. Kwon, D. Kim, J.H. Park,** Nano Lett., 2017, 17, 2028.

[179] **T. Bu, X. Liu, Y. Zhou, J. Yi, X. Huang, L. Luo, J. Xiao, Z. Ku, Y. Peng, F. Huang, Y.-B. Cheng, J. Zhong,** Energy Environ. Sci., 2017, 10, 2509.

[180] **T.J. Jacobsson, J.-P. Correa-Baena, E.H. Anaraki, B. Philippe, S.D. Stranks, M.E.F. Bouduban, W. Tress, K. Schenk, J. Teuscher, J.-E. Moser, H. Rensmo, A. Hagfeldt,** J. Am. Chem. Soc., 2016, 138, 10331.

[181] **V. Kumar, J. Barbe, W. L. Schmidt, K. Tsevas, B. Ozkan, C.M. Handley, C.L. Freeman, D.C. Sinclair, I.M. Reaney, W.C. Tsoi, A. Dunbar, C. Rodenburg,** J. Mater. Chem. A, 2018, 6, 23578.

[182] **Y. Luo, S. Aharon, M. Stuckelberger, E. Magaña, B. Lai, M.I. Bertoni, L. Etgar, D.P. Fenning,** Adv. Funct. Mater., 2018, 28, 1706995.

[183] **Q. Ma, S. Huang, S. Chen, M. Zhang, C.F.J. Lau, M.N. Lockrey, H.K. Mulmudi, Y. Shan, J. Yao, J. Zheng, X. Deng, K. Catchpole, M.A. Green, A.W.Y. Ho-Baillie,** J. Phys. Chem. C, 2017, 121, 19642.

[184] **Q. Chen, H. Zhou, T.-B. Song, S. Luo, Z. Hong, H.-S. Duan, L. Dou, Y. Liu, Y. Yang,** Nano Lett., 2014, 14, 4158.

[185] **L. Wang, C. McCleese, A. Kovalsky, Y. Zhao, C. Burda,** J. Am. Chem. Soc., 2014, 136, 12205.

[186] **J. Haruyama, K. Sodeyama, L. Han, Y. Tateyama,** J. Phys. Chem. Lett., 2014, 5, 2903.

[187] **A. Buin, P. Pietsch, J. Xu, O. Voznyy, A.H. Ip, R. Comin, E.H. Sargent,** Nano Lett., 2014, 14, 6281.

[188] **Z. Song, S.C. Watthage, A.B. Phillips, B.L. Tompkins, R.J. Ellingson, M.J. Heben,** Chem. Mater., 2015, 27, 4612.

[189] **H. Choi, J. Jeong, H.B. Kim, S. Kim, B. Walker, G.H. Kim, J.Y. Kim,** Nano Energy, 2014, 7, 80.

[190] **Z. Li, M. Yang, J.-S. Park, S.-H. Wei, J.J. Berry, K. Zhu,** Chem. Mater., 2016, 28, 284.

[191] **Z. Xu, L.g Zeng, J. Hu, Z. Wang, P. Zhang, C.J. Brabec, K. Forberich, Y. Mai, F. Guo,** Nano Energy, 2022, 91, 106658.

[192] **N.J. Jeon, J.H. Noh, Y.C. Kim, W.S. Yang, S. Ryu, S. Il Seok,** Nat. Mater., 2014, 13, 897–903.

[193] **L. Chao, T. Niu, W. Gao, C. Ran, L. Song, Y. Chen, W. Huang,** Adv. Mater., 2021, 33, 2005410.

[194] **F. Matteocci, S. Razza, F. Di Giacomo, S. Casaluci, G. Mincuzzi, T.M. Brown, A. D'Epifanio, S. Licoccia, A. Di Carlo,** Phys. Chem. Chem. Phys., 2014, 16, 3918.

[195] **S. Razza, F. Di Giacomo, F. Matteocci, L. Cina, A. L. Palma, S. Casaluci, P. Cameron, A. D'epifanio, S. Licoccia, A. Reale,** J. Power Sources, 2015, 277, 286.

[196] **J. Seo, S. Park, Y.C. Kim, N.J. Jeon, J.H. Noh, S.C. Yoon, S.I. Seok,** Energy Environ. Sci., 2014, 7, 2642.

[197] **J.H. Heo, H.J. Han, D. Kim, T.K. Ahn, S.H. Im,** Energy Environ. Sci., 2015, 8, 1602.

[198] **A. Priyadarshi, L.J. Haur, P. Murray, D. Fu, S. Kulkarni, G. Xing, T.C. Sum, N. Mathews, S.G. Mhaisalkar,** Energy Environ. Sci., 2016, 9, 3687.

[199] **Y. Wang, T. Wu, J. Barbaud, W. Kong, D. Cui, H. Chen, X. Yang, L. Han,** Science, 2019, 365, 687–691.

[200] **Y. Hu, S. Si, A. Mei, Y. Rong, H. Liu, X. Li, H. Han,** Solar RRL, 2017, 1, 1600019.

[201] **K. Inzani, M. Nematollahi, F. Vullum-Bruer, T. Grande, T.W. Reenaas, S.M. Selbach,** Phys. Chem. Chem. Phys., 2017, 19, 9232–9245.

[202] **J. Tirado, M. Vásquez-Montoya, C. Roldán-Carmona, M. Ralaiarisoa, N. Koch, M.K. Nazeeruddin, F. Jaramillo,** ACS Appl. Energy Mater., 2019, 2, 4890–4899.

[203] **H. Guo, X. Huang, B. Pu, J. Yang, H. Chen, Y. Zhou, J. Yang, Y. Li, Z. Wang, X. Niu,** RSC Adv., 2017, 7, 50410–50419.

[204] **R. Cheacharoen, N. Rolston, D. Harwood, K.A. Bush, R.H. Dauskardt, M.D. Mc Gehee,** Energy Environ. Sci., 2018, 11, 144–150.

[205] **A. Extance,** Nature, 2019, 570, 429–432.

INFORMATION ABOUT AUTHORS

Mohammad KHAJA NAZEERUDDIN – *Group for Molecular Engineering of Functional Materials, Institute of Chemical Sciences and Engineering, École Polytechnique Fédérale de Lausanne (EPFL).*

Maria VASILOPOULOU – *Institute of Nanoscience and Nanotechnology, National Centre for Scientific Research Demokritos.*